Model development of dust emission and heterogeneous chemistry within the Community Multiscale Air Quality modeling system and its application over East Asia

Xinyi Dong[1], Joshua S. Fu[1], Kan Huang[1], Daniel Tong[2,3,4]

[1]Department of Civil and Environmental Engineering, the University of Tennessee, Knoxville, TN 37996, USA

[2]NOAA/OAR/ARL, NOAA Center for Weather andd Climate Prediction, College Park, MD 20740, USA

[3]Center for Spatial Information Science and Systems, George Mason University, Fairfax VA 22030, USA

[4]Cooperative Institute for Climate and Satellites, University of Maryland, College Park, MD 20740, USA

* Correspondence to: Joshua S. Fu (jsfu@utk.edu)

Abstract

The Community Multiscale Air Quality (CMAQ) model has been further developed in terms of simulating natural wind-blown dust in this study, with a series of modifications aimed at improving the model's capability to predict the emission, transport, and chemical reactions of dust. The default parameterization of initial threshold friction velocity constants in the CMAQ are revised to avoid double counting of the impact of soil moisture by re-analysis of field experiment data; source-dependent speciation profiles for dust emission are derived based on local measurements for the Gobi and Taklamakan deserts in East Asia; and dust heterogeneous chemistry is also implemented. The improved dust module in the CMAQ is applied over East Asia for March and April from 2006 to 2010. Model evaluation result shows that the simulation bias of PM_{10} and aerosol optical depth (AOD) is reduced from -55.42% and -31.97% by the original CMAQ to -16.05% and -22.1% by the revised CMAQ, respectively. Comparison with observations at the nearby Gobi stations of Duolun and Yulin indicates that applying a source-dependent profile helps reduce simulation bias for trace metals. Implementing heterogeneous chemistry also results

in better agreement with observations for sulfur dioxide (SO_2), sulfate (SO_4^{2-}), nitric acid (HNO_3), nitrous oxides (NO_x), and nitrate (NO_3^-). Investigation of a severe dust storm episode from 19 to 21 March 2010 suggests that the revised CMAQ is capable of capturing the spatial distribution and temporal variation of dust. Model evaluation also indicates potential uncertainty within the excessive soil moisture used by meteorological simulation. The mass contribution of fine mode particles in dust emission may be underestimated by 50%. The revised CMAQ model provides a useful tool for future studies to investigate the emission, transport, and impact of wind-blown dust over East Asia and elsewhere.

.

1. Introduction

Natural dust has a wide impact on many different aspects of the Earth's system. It reduces atmospheric visibility (Engelstaedter et al., 2003; Kurosaki and Mikami, 2005; Washington et al., 2003), deteriorates air quality (De Longueville et al., 2010; Prospero, 1999), alters the radiative forcing budget (Liao et al., 2004; Miller et al., 2006; Reddy et al., 2005), and also affects the cloud properties and precipitation (Rosenfeld et al., 2001; Forster et al., 2007). Over East Asia, spring time dust storms often lead to severe air pollution since the intensively elevated aerosol loadings are dumped over the most populated areas. The estimated global source of mineral dust with diameters below 10μm is between 1,000 and 4,000 Tg/year on a global scale as reported by Intergovernmental Panel on Climate Change (IPCC), and Zhang et al. (2003) reported annual Asian dust emission as 800 Tg. East Asian dust mainly originates from two dominant source regions and their surrounding areas, including the Taklamakan Desert in northwest China and the Gobi Desert in Mongolia and northern China (Huang et al., 2010). In spring, the Mongolian Cyclone associated with the East Asian trough often leads to strong northwesterly near surface winds (Shao and Dong, 2006) that lift and transport the eolia dust particles. East Asian dust can transport to densely populated areas over China (Qian et al., 2002), South Korea (Chun et al., 2001; Park and In, 2003), and Japan (Ma et al., 2001; Uno et al., 2001), and at times can even transport across the Pacific Ocean, reaching as far as the west coast of North America (Fairlie et al., 2010; Wang et al., 2012; Zhao et al., 2010). Along the transport pathway, mineral dust

particles also serve as carriers and reaction platforms by uptaking reactive gases such as ozone (O_3), nitrogen oxides (NO_x), sulfur dioxide (SO_2), nitric acid (HNO_3), hydroxyl radicals (OH), and volatile organic compounds (VOCs). The dust heterogeneous chemistry may change the photochemistry, acid deposition, and production of secondary aerosols in the atmosphere. Besides, East Asian dust is believed to contribute geochemically significant amounts of minerals that are deposited into the western part of the Pacific Ocean. These minerals may alter the oceanic primary productivity (Zhang et al., 2003; Zhuang et al., 1992) as well.

Since natural dust links the biogeochemical cycle of land, atmosphere, and ocean, understanding the emission, evolution, and transport of dust is essential for further examining its impacts on the Earth's system. Numerical modeling is one of the most important approaches for systematically investigating dust. Many global models simulate dust emissions, transport, and depositions. Huneeus et al. (2011) conducted intercomparisons of 15 global models and reported their simulated aerosol optical depth (AOD) and Angström Exponent (AE) within a factor of two and the total deposition and surface concentration within a factor of 10 with respect to observations, indicating significant variations among different models. Regional models usually represent dust by following a coherent manner as global models. For example, the WRF-Chem (Grell et al., 2005) coupled with the GOCART scheme (Ginoux et al., 2001) has been applied to simulate dust emission over Middle-East Asia (Kumar et al., 2014), the United States (Zhao et al., 2010), and East Asia (Chen et al., 2013). The STEM (Carmichael et al., 2003) used the COAMPS scheme (Liu and Westphal, 2001) and has been applied over East Asia (Tang et al., 2004). Regional models have fine spatiotemporal resolution and multiple physical parameterizations at the cost of intensive computation. As compared to global models, regional models may provide more realistic representations of the surface roughness, soil moisture and contents, and also allow comparable validation against surface observations (Darmenova and Sokolik, 2008).

The Community Multiscale Air Quality (CMAQ) model is a state-of-science model and has been applied in numerous regional modeling studies worldwide. Unlike other models in which dust is usually treated as a unique aerosol, the CMAQ distributes dust particles into 19 aerosol species, such as inorganic aerosols and trace metals. This approach is

consistent with the original design of the CMAQ as an air quality model, and it also provides a potential platform to examine the diversities of chemical and physical properties within dust particles. It enables the model to examine the mixing status and net effect of natural dust and anthropogenic aerosols on air quality and regional climate. The validation of the CMAQ performance is not well understood due to limited research efforts. Appel et al. (2013) conducted a full year simulation with CMAQ over the continental United States for 2006, and reported good agreement between simulations and observations, with the mean bias around $\pm 0.5 \mu g/m^3$ and $0.5\text{-}1.5 \mu g/m^3$ (~±30%) for soil concentrations over western and eastern United States, respectively. But the CMAQ simulations over other regions underestimate dust emissions significantly. Fu et al. (2014) reported that the default dust scheme in the CMAQ underestimated dust emission by 98% during a six-day dust storm episode in 2011. With the modeling domain covering the entire Northern Hemisphere, Xing et al. (2015) also suggested that the CMAQ underestimated AOD by 30%-60% in areas where dust is dominant, while the bias was less than ±15% elsewhere.

The studies mentioned above indicate that the capability of the CMAQ for simulating natural dust emissions remains poorly understood. In addition, the current dust scheme in the CMAQ does not include dust heterogeneous chemistry, while some studies have revealed the important impact of dust chemistry on ambient air pollutants with both measurement (Krueger et al., 2004; Matsuki et al., 2005; Usher et al., 2003) and modeling evidence (Bauer et al., 2004; Bian and Zender, 2003; Dentener et al., 1996). The objective of this study is to evaluate and improve the model's capability of reproducing dust emission, and also enable the model to treat the dust heterogeneous chemistry. Section 2 introduces the method of applying new parameterizations and implementing dust heterogeneous chemistry into the CMAQ, whereas Section 3 summarizes the improved model performance. Section 4 discusses the enhanced model capability and remaining uncertainties, and Section 5 concludes the paper with a summary of the findings.

2. Methodology

2.1 Improvement of the CMAQ wind-blown dust emission module

The process of wind-blown dust emission is controlled by a number of environmental variables, including wind speed, soil texture, land use type, vegetation cover, and soil moisture. Dust deflation is favored by dry soil with low and sparse vegetation and constrained by high soil moisture. The dust emission scheme employed in the CMAQ is developed by Tong et al. (2015). The emission (vertical flux) of the dust F (g/m^{2}s) was estimated based on a modified Owen's equation (Owen et al., 1964; Tong et al., 2015):

$$F = \sum_{i=1}^{M}\sum_{j=1}^{N} K \times A \times \frac{\rho}{g} \times S_i \times SEP \times u_* \times (u_*^{\,2} - u_{*ti,j}^{\,2}) \qquad \text{for } u_* > u_{*ti,j} \tag{1}$$

where M is the erodible land use type, N is the soil texture type, K is the ratio of vertical to horizontal flux calculated based on the amount of clay (*clay%*) within the soil:

$$K = \begin{cases} 10^{0.134\times(clay\%)-6}, when: clay\% < 20\% \\ 0.0002, when: clay\% \geq 20\% \end{cases} \tag{2}$$

A is a scaling factor, ρ is air density, g is gravitational acceleration (9.8 m/s^2), S_i is dust source area for land type i, SEP is the soil erodibility factor, which is calculated based on the fraction of clay, silt, and sand of the soil as:

$$SEP = 0.08 \times clay + 1.0 \times silt + 0.12 \times sand \tag{3}$$

u_* is the friction velocity, and $u_{*ti,j}$ is the threshold friction velocity for soil type j and land use type i. More details of the dust emission algorithm have been given in Tong et al. (2015). Equation (1) is applied only when the model calculated friction velocity exceeds the designated threshold value. Therefore, the value of threshold friction velocity is critical to determine the onset and magnitude of dust emission in the CMAQ model.

In the CMAQ dust module, the threshold friction velocity is dynamically calculated based on the presence of non-erodible elements and the change of soil moisture (Tong et al., 2015). The effect of non-erodible elements is represented by wind energy partitioning following Marticorena et al. (1997). The effect of soil moisture on dust emission is implemented following a two-step approach proposed by Fecan et al. (1999). First, the

maximum water holding capacity (W_{max}) for each soil type is determined based on the amount of clay in the soil:

$$W_{max} = (0.0014 \times clay\% + 0.17) \times clay\% \quad (4)$$

In case that soil moisture exceeds W_{max}, the threshold friction velocity is then adjusted as:

$$u_{*ti,j} = u_{*ci,j} \times Z_{i,j} \times f_{soilm\ i,j} \quad (5)$$

where $u_{*ci,j}$ is the initial threshold friction velocity constant, $Z_{i,j}$ is the surface roughness adjusting factor calculated with surface roughness length from the meteorology field, and $f_{soilm\ i,j}$ is the moisture adjustment factor calculated using a revised Fecan formulation (Fecan et al., 1999) as:

$$f_{soilm\ i,j} = \begin{cases} 1.0, \textit{ for } S_m \le W_{max} \\ \left(1.0 + 1.21 \times (S_m - W_{max})^{0.68}\right)^{0.5}, \textit{ for } W_{max} < S_m \le S_l \end{cases} \quad (6)$$

where S_m is soil moisture, and S_l is the saturation soil moisture limit determined by soil textures.

Previously, the values of initial threshold friction velocity constant were taken from observed data from wind tunnel experiments conducted by Gillette and co-workers (Gillette et al., 1980, 1982). Fu et al. (2014) reported the $u_{*ci,j}$ used in the CMAQ has an average value of 0.7m/s among all soil types, which is too high to generate enough dust particles over East Asia. Fu et al. (2014) used a fixed value of 0.3m/s based on a study of local measurements in a northern desert in China (Li et al., 2007). Although this smaller threshold helps generate higher production of dust emission during the six-day simulation episode from 1 to 6 May 2011, the arbitrarily designated threshold value for all land covers and soil categories prevents the model from reproducing spatial and temporal variations of dust emission. In this study, we have conducted a reanalysis of the field data (Gillette et al., 1980, 1982) and revised the threshold friction velocities through removing the double counting of soil moisture in the CMAQ dust emission modeling. In these field campaigns, some of these experiments were performed under rather dry conditions, but for other samples the effect of soil moisture cannot be ignored. Therefore, these values reported from field experiments are not always suitable for being used directly as the initial threshold

friction velocity constant, which is assumed to represent extremely dry conditions. Meanwhile, in the CMAQ dust module, dynamic soil moisture data are used to adjust threshold friction velocity. Therefore, we need to convert the wet-condition data into threshold values under dry conditions. Otherwise, there will be double counting of soil moistures under some cases.

We took a three-step approach to calibrate the threshold friction velocity. First, the value of soil moisture was extracted for each sample from the raw field dataset (courtesy from Dale Gillette, retired). Next, these data were used to feed the Fecan formula (Fecan et al. 1999) to derive the dry-condition threshold velocity by casting soil moisture back to zero. We have reprocessed the data for the soil and land use types measured by Gillette 1980 and 1982. In case of missing data for certain soil types, we have chosen the values with the soil composition closest to a measured type following the USDA soil composition diagram (Fig 1 of Gillette 1980). Finally, the revised values of $u_{*ci,j}$ are implemented into the CMAQ. Comparison of the default and revised constants are summarized in Figure 1 (c). As the double-count of soil moisture has been corrected, the revised constants are lower than the default ones. The majority of land cover in the Gobi is categorized as shrub land, where the revised initial threshold friction velocity constants are significantly lower than the default values for all soil types as shown in Fig. 1 (c), indicating that the revised scheme is expected to produce higher dust emissions over the Gobi. The Taklamakan Desert is mainly configured as barren or sparsely vegetated land cover with sandy soil type, which only shows a small drop of the threshold friction velocity constant from 0.28m/s to 0.23m/s, indicating that the changes of dust emission over the Taklamakan may not be substantial. The CMAQ distributes dust emission to four size bins: 0.1-1.0μm, 1.0-2.5μm, 2.5-5.0μm, and 5.0-10.0μm with the mass contribution as 3%, 17%, 41%, and 39% within each bin, respectively. The first two bins represent the fine mode aerosol and the larger two represent the coarse mode. So the mass contribution is 20% for fine mode 80% for coarse mode aerosol.

2.2 Implementing source-dependent speciation profile

The emission of natural wind-blown dust particles is distributed to 19 aerosol species in the CMAQ following the profile developed based on the EPA's SPECIATE database

(Simon et al., 2010). As compared with other models that treat dust as a unique aerosol species, the CMAQ approach provides a more detailed description of the chemical components of dust. However, mass contributions of different chemical components may differ greatly among different source areas, thus using a fixed profile for all dust sources may introduce uncertainty and lose the capacity of modeling the varieties of dust particles. The mass contribution of Aluminum (Al) is around 5%~8% for pure minerals around the world, and the ratios between other trace metals and Al may vary substantially for different dust particles. Thus the elemental mass ratio between Calcium and Aluminum (Ca/Al) is usually used to identify the source of dust samples (Huang et al., 2010; Sun et al., 2005). For example, the Ca/Al ratio for Saharan dust is around 0.9 and 1.0 for fine and coarse dust particles, respectively (Blanco et al., 2003; Formenti et al., 2003; Kandler et al., 2007; Reid et al., 2003); for Arabian dust is around 0.13 and 0.15 for coastal and inland dust, respectively (Krueger et al., 2004); for Taklamakan dust is about 1.5~1.9 (Huang et al., 2010); and for dust from the Gobi Desert is 0.4~1.1 (Arimoto et al., 2006; Zhang et al., 2003). To characterize the dust aerosols in the CMAQ better, source-dependent speciation profiles are developed in this study for the Gobi and Taklamakan deserts based on local measurement data collected by Huang et al. (2010). These two profiles are compared with the default one in the CMAQ as shown in Table 1. For the model species which are not measured in Huang et al. (2010), including primary organic carbons (APOC), non-carbon aerosols (APNCOM), elementary carbons (EC), silicon (ASI), and water (AH2O), their values for the Taklamakan and Gobi are kept the same as in the default profile. And for unspeciated (AOTHR) and non-anion dust (ASOIL), their values in the two new profiles are calculated based on the contributions of all other species, to keep the total mass contributions conservative. It is important to notice that the model species refer to an anion or cation phase for sulfate (ASO4, SO_4^{2-}), nitrate (ANO3, NO_3^-), chloride (ACL, Cl^-), ammonium (ANH4, NH_4^+), sodium (ANA, Na^+), Ca_2^+ (ACA), magnesium (AMG, Mg_2^+), and potassium (AK, K^+), and an element phase for iron (AFE, Fe), Al(AAL), silicon (ASI, Si), titanium (ATI, Ti), and manganese (AMN, Mn). Mass contributions of different aerosols differ significantly among the profiles as shown in Table 1. For example, Ca_2^+ accounts for 7.94% of the total fine particle mass in the default profile, which is much higher than the Taklamakan (2.063%) and the Gobi (1.788%). For Mg_2^+, the default profile

assumes a zero percentage of mass contribution, yet the values for the Taklamakan and Gobi are 0.165% and 0.799%, respectively. The K^+ contribution within the default profile is 3.77%, while the Taklamakan is 0.153% and the Gobi is 0.282%. Si is one of the most abundant metals in the crust, yet the default speciation profile has an inappropriate assumption as zero Si content in coarse mode dust particles. As no measurements are found for Si over the Taklamakan or Gobi, we use the element ratio of Al/Si as 8%/28% to derive the mass contribution of Si in the coarse model, which is a conventional approach for trace metal analysis (Huang et al., 2010). Different configurations within the speciation profile will lead to significant differences of model predictions for these trace metals, demonstrated in more detail in Section 3.

2.3 Implementation of heterogeneous reactions

The default heterogeneous chemistry scheme within the CMAQ considered the conversions from N_2O_5 to HNO_3, and from NO_2 to HONO and HNO_3. These reactions play an important role in the nighttime production of nitrate aerosols (Dong et al., 2014; Pathak et al., 2011; Pun and Seigneur, 2001). Heterogeneous reactions are treated as irreversible in the model (Davis et al., 2008; Sarwar et al., 2008; Vogel et al., 2003). While dust particles serve as a platform for heterogeneous reaction, they also participate in some of the reactions to uptake the gas-phase species. The uptake of gases onto the surface of dust particles is defined by a pseudo-first-order reaction rate *K* (Dentener et al., 1996; Heikes and Thompson, 1983) calculated as:

$$K = \left(\frac{r_p}{D_g} + \frac{4}{v_g \gamma_g} \right)^{-1} A_p \quad (7)$$

where r_p is the radius of the particle, D_g is the diffusion coefficient of gas molecules, v_g is the mean molecular velocity of gas, A_p is the surface area of the particle, and γ_g is the uptake coefficient for gas. Many research efforts have been devoted to quantify the uptake coefficients. The reported values of the uptake coefficient may differ by more than 2-3 orders of magnitude, depending on the source of the dust samples and analytical methods (Cwiertny et al., 2008; Usher et al., 2003). While this work focuses on East Asia, the uptake coefficients are mainly collected from Zhu et al. (2010), which summarized the estimations

for dust samples from deserts in China. The "best guess" of uptake coefficients were suggested based on the analysis of different measurement studies summarized in Zhu et al. (2010). But in this study both the lower and upper limits of uptake coefficients are examined to evaluate their impacts. Table 2 lists the 13 dust heterogeneous reactions implemented into the CMAQ in this study, with the lower and upper boundaries of uptake coefficients.

2.4 Model inputs, configuration, and simulation scenarios

The CMAQ model simulation uses version 5.0.1. In this study, the CMAQ is configured with the updated 2005 carbon bond gas-phase mechanism (CB05), aerosol module AE6, in-line photolysis calculation and NO emission from lightning, and the Euler backward iterative (EBI) solver. The modeling domain covers East Asia and Peninsular Southeast Asia as shown in Figure 2. The CMAQ simulation is performed with a 36km horizontal grid spacing and 34 vertical layers with a model top as 50hPa, with finer resolution at the near surface layers to represent clearly the planetary boundary layer. Simulation period covers March and April from 2006 to 2010 to represent the spring dust episode of East Asia.

The meteorology field is simulated with the Weather Research and Forecasting model (WRFv3.4, Skamarock et al., 2008). Initial and boundary conditions are downscaled from the GEOS-Chem global model with the same simulation period as CMAQ from 2006 to 2010, and the downscaling method is described in Lam and Fu (2009). Biogenic emission is from MEGAN2.1 (Guenther et al., 2006; Muller et al., 2008), biomass burning emission is from FLAMBE (Reid et al., 2009), and anthropogenic emission is from Zhao et al. (2013) over China and INTEX-B over other countries within the domain. More details about meteorology and emission datasets are described in Dong and Fu (2015a, b).

To examine the performance of the CMAQ model development with revised parameterization and dust heterogeneous reactions, a total of six scenarios are conducted as listed in Table 3. The simulations Dust_Off and Dust_Default are designed to investigate performance of the CMAQ without dust emission and with the default dust plume rise scheme; Dust_Revised is designed to investigate the performance of applying the new parameterization of initial friction velocity threshold constants; Dust_Profile is designed to

examine the improvement by applying source-dependent dust composition profiles; and Dust_Chem and Dust_ChemHigh are designed to examine the impacts of implementing heterogeneous chemistry with lower and upper estimations of uptake coefficients, respectively. The scenario Dust_Profile, Dust_Chem, and Dust_ChemHigh are all performed based on Dust_Revised.

2.5 Observations

Both ground-based measurements and satellite observations are used in this study to help examine the uncertainty and evaluate the performance of the model. The Air Pollution Index (API, http://datacenter.mep.gov.cn) reported by the Chinese Ministry of Environmental Protection (MEP) is used to evaluate the PM_{10} predictions from the CMAQ. The API is reported on a daily basis with a national coverage of 86 middle size or larger cities in China and has been applied in many modeling studies for evaluation purposes (Zhao et al., 2013). To investigate the transport of dust particles over downwind areas simulated by the model, we also used surface observations from the Acid Deposition Monitoring Network in East Asia (EANET; EANET, 2007) over Japan, and observations from the Taiwan Air Quality Monitoring Network (TAQMN; http://taqm.epa.gov.tw/taqm/en/default.aspx). EANET provides hourly or daily records of PM_{10}, O_3, NO_x, and SO_2, and also bi-weekly (or longer interval) records of HNO_3, SO_4^{2-}, and NO_3^-. Data from EANET is also employed in this study for examining model performance with dust heterogeneous chemistry. The TAQMN provides observations of most criteria air pollutants yet only PM_{10} observations at the Xinzhuang site are used in this study to focus on dust storm impact. These variables are used to examine the simulation responses by implementing dust heterogeneous chemistry. Ground-based measurements of K^+, Mg_2^+, Ca_2^+, and $PM_{2.5}$ at Duolun and Yunlin from Fudan University's observation network (Huang et al., 2010) are used to investigate the model's capability of simulating tracer metals by applying the source-dependent speciation profile for suspended dust particles. AOD from the AErosol RObotic NETwork (AERONET; http://aeronet.gsfc.nasa.gov/) operated by NASA is also collected to evaluate the CMAQ predictions. To examine the spatial distribution and column density of model-simulated dust particles, we also used AOD products from the Moderate Resolution Imaging Spectroradiometer (MODIS; http://modis.gsfc.nasa.gov/). The locations of observational

stations by the API, EANET, TAQMN, and AERONET are indicated in Figure 2, along with the locations of Duolun and Yunlin. Table 4 summarizes the detailed information of each observation network. All observations are collected for the period of March and April from 2006 to 2010, except for the Fudan Univ. data which only covers March and April in 2007.

3. Results

3.1 Improved model performance with revised friction velocity thresholds

To examine model improvement by implementing new initial threshold friction velocity constants, simulation results from Dust_Default and Dust_Revised are compared for the spatial distribution of PM_{10} and evaluation bias against API. Dust_Default - Dust_Off, and Dust_Revised - Dust_Off represents the PM_{10} from the default dust scheme and the revised dust scheme, respectively, as shown in Figures 3 (a) and (b). PM_{10} concentrations generated from dust are averaged for March and April from 2006 to 2010. Figure 3 (a) indicates that the default dust scheme produces a very limited amount of PM_{10} only over the Gobi Desert for less than 70μg/m^3, which can hardly represent the East Asian dust storms. The revised scheme produces higher PM_{10} concentrations as more than 400μg/m^3 at the Gobi source region, as shown in Figure 3(b). Dust plumes are generated by the revised model over the Gobi and Taklamakan deserts, and also from sparse grassland over the northwest region of the Tibetan Plateau. Particles from dust plumes are transported southeastwardly and contributed 50~100μg/m^3 of PM_{10} over northern and eastern China, and less than 50μg/m^3 over southern China, South Korea, and Japan. Huang et al. (2010) demonstrated that there are two transport pathways for Asian dust: plumes from the Gobi and Taklamakan are either pushed by prevailing winds eastward towards South Korea and Japan or southeastward down towards southern China and Taiwan. With the revised dust scheme, the CMAQ generally reproduces the spatial distribution of Asian dust as shown in Figure 3(b), which indicates the most significant impact over northern and eastern China and relatively weak impacts over downwind areas along the transport pathway towards southeast. Figures 3 (c) and (d) demonstrate the evaluation bias at the API cities over China for the Dust_Default and Dust_Revised scenarios, respectively. With the default dust

scheme, the CMAQ shows a large negative bias for the entire domain. Most serious underestimation is found over northern and western China, with a negative bias more than -80μg/m^3. Figure 3(c) also suggests that cities closer to the Taklamakan and Gobi deserts have larger negative bias, indicating that the default scheme cannot generate sufficient dust emission to reproduce the observed PM_{10}. With the revised scheme as shown in Figure 3 (d), simulation biases for most of the cities are reduced down to ±20μg/m^3. The largest overestimation is found at Hohhot as 39μg/m^3, and he largest underestimation is found at Xining and Lanzhou (-60μg/m^3). Figure 3(d) also indicates that model tend to have larger simulation discrepancy in cities close to the desert.

Figures 4 (a) to (c) summarizes the evaluation statistics for simulated PM_{10} against observations from the API. Daily data pairs from observation and simulation are used here to calculate the statistics. The Dust_Off scenario underestimates PM_{10} concentration by -56.74%. Since dust storms from the Taklamakan and Gobi substantially contribute to suspended particle concentrations over East Asia during spring, simulation with no dust emission should be responsible for the large underestimation. With the default dust emission module, model performance for the scenario Dust_Default is only slightly improved and PM_{10} is still underestimated by -55.42%, as shown by Figure 4(b). The comparison between Dust_Off and Dust_Default suggests that the default dust module is not able to generate sufficient elevated particles to match the observed PM_{10} levels from the API. On the other hand, the Dust_Revised scenario shows a much better performance with a NMB value of -16.06% as shown in Figure 4(c). Simulation results are also evaluated against AOD observations from the AERONET, with the statistics shown in Figures 4 (d) to (f). Statistics for AOD evaluation against the AERONET suggest similar model performances as for PM_{10}. The CMAQ simulation without dust rise underestimates AOD by -31.34% at AERONET stations, and the default dust module has almost no improvement for AOD prediction. The Dust_Revised scenario underestimates AOD by -22.1%, indicating that the revised scheme is also able to improve the model performance for simulating fine mode dust.

3.2 Impacts of applying source-dependent profile

Speciation of dust particles determines the contributions of crust species and trace metal concentrations predicted by the model. As described in Section 2.2, we modified the fixed speciation profile within the CMAQ to be source-dependent for the Gobi and Taklamakan, respectively, and in this section ground-based observations collected at Duolun and Yulin are used to investigate the impacts by applying different speciation profiles. The model simulations from the Dust_Revised and Dust_Profile scenarios are compared with observations for K^+, Mg_2^+, and Ca_2^+ with data pairs, as shown in Figure 5 (simulations and observations for K^+ and Mg_2^+ are upscaled by 5 and 10 times, respectively, to make them comparable with Ca_2^+ in the same figure), and evaluation statistics are summarized in Table 5. The two cities are close to the Gobi Desert, as shown by Figure 2. Huang et al. (2010) used back trajectory and Ca/Al ratio analysis to demonstrate that the Gobi Desert is the main contributor for dust particles at Duolun and Yulin. Figure 5(a) indicates that with the default speciation profile, the CMAQ overestimates K^+ and Ca_2^+ by 208.9% and 36.69%, respectively. Predicted Mg_2^+ concentration is almost zero because there is no emission of Mg_2^+ in the anthropogenic emission inventories, and the default profile indicated zero percentage mass contribution of Mg_2^+ from dust emission. With the source-dependent speciation profile, the CMAQ simulation of Mg_2^+ is increased significantly as shown in Figure 5(b). The revised CMAQ underestimates K^+ and Ca_2^+ by -47.83% and -53.12%, respectively. Consistent negative bias for trace metals should due to the underestimation of total fine mode aerosol within dust. Figure 5(c) shows the comparison between observed and simulated $PM_{2.5}$ concentrations at Duolun and Yulin. The Dust_Revised and Dust_Profile scenarios only differ in terms of their speciation profile for particles. The predicted $PM_{2.5}$ from the two scenarios are almost identical, so simulation from only Dust_Profile is shown in Figure 5(c). On the one hand, concentration of $PM_{2.5}$ is underestimated by -45.59%, which is consistent with the underestimations of Mg_2^+, K^+, and Ca_2^+. On the other hand, simulation bias shown in Figure 3(d) suggests a slight overestimation of PM_{10} at cities close to the Gobi Desert. So it is highly possible that fine particle mass contribution configured within the CMAQ might be underestimated. Unfortunately, measurements made by Huang et al. (2010) only collected data for total suspended particles (TSP) and no PM_{10} observation is found for Duolun or Yulin. The

comparison between the Dust_Revised and Dust_Profile scenario suggests that the source-dependent speciation profile is more reasonable for predicting trace metals from dust emission.

3.3 Impacts of heterogeneous chemistry

Dust heterogeneous chemistry involves uptake of gas-phase species and production of secondary inorganic aerosols. In this section we investigate the impacts of implementing dust chemistry into the CMAQ by examining the simulation difference between Dust_Chem and Dust_Profile, and the difference between Dust_ChemHigh and Dust_Profile. Figure 6 shows the concentration changes (color contours represent the absolute concentration changes, and dash lines represent the percentage changes) under heterogeneous chemistry with lower (left column) and upper (right column) limits of uptake coefficients for O_3 (1st row), SO_2 (2nd row), SO_4^{2-} (3rd row), HNO_3 (4th row), NO_x (5th row), and NO_3^- (6th row). All variables are averaged for March and April from 2006 to 2010. The spatial distributions shown in Figure 6 suggest that impacts of dust chemistry are more pronounced in eastern China over the downwind areas than in the dust source area near the deserts. This is because eastern China has intense anthropogenic emissions that help to accelerate the dust chemistry, while the desert areas in northern and western China have much lower concentrations of the reactive gases. Dong and Fu (2015a) reported that in spring, O_3 concentration is around 30ppbv and less than 5ppbv for NO_2 and SO_2 over the Gobi, while the concentrations over eastern China are 50~60ppbv for O_3 and 10~40ppbv for NO_2 and SO_2. More abundance of these reactive gases participate in the heterogeneous reactions on the surface of dust particles transported from deserts, and thus lead to a more significant impact of dust chemistry over the downwind area instead of over the deserts. Li et al. (2012) also reported that the impact of dust chemistry for O_3, SO_2, and NO_2 is less than 5% over the Gobi but up to 30~40% in eastern China and even higher over the western Pacific. O_3 concentration is reduced by 3~6 ppbv (2%~10%) and 5~11ppbv (4%~20%) with the lower and upper limits of uptake coefficients, respectively, due to irreversible reaction R1 as listed in Table 2, which agrees well with the values reported by Tang et al. (2004) as 20% and Li et al. (2012) as 5%~20%. Wang et al. (2012) reported lower O_3 reduction due to dust chemistry by 3.8ppbv and 7.3ppbv with lower and upper uptake coefficients, respectively, which could be because of using a different simulation

year (2001) with a lower baseline O_3 over East Asia. Concentration of SO_2 is reduced by ~2 ppbv (10%) and ~6 ppbv (30%) with lower and upper limits of uptake coefficients, respectively, due to the consumption in reaction R13, which also leads to the increase of SO_4^{2-} concentration by ~3μg/m^3 (8%) and more than 5μg/m^3 (15%) under Dust_Chem and Dust_ChemHigh, respectively. Impacts on SO_2 reported by other studies have a moderate difference with a factor of 2 or more, varying from 55% by Tang et al. (2004) as the highest, 10%~20% as the medium (Li et al., 2012), and 5%~8% as the lowest (Wang et al., 2012). Different impacts caused by heterogeneous chemistry reported by different studies should mainly be attributed to the different simulation episodes. Tang et al. (2004) focused on dust episodes only in 2001 with lower baseline pollutants from anthropogenic emission, Li et al. (2012) also simulated dust episodes but in 2010, and Wang et al. (2012) simulated 2001 but focused on the entirety of April, where the monthly averages of particles are apparently smaller than values from dust episodes only. Reaction R7 indicates consumption and R11 indicates production of HNO_3, while the net effect of dust chemistry is found to decrease HNO_3 concentration by 0.2ppbv~0.8ppbv (8%~30%) as shown in Figures 6(e) and (f). Our result is comparable with the values reported by Li et al. (2012) as 5%~40%, but smaller than that reported by Tang et al. (2004) as 30%~70%. Although the reaction R9 indicates uptake of NO_x by dust particles, simulation results suggest that NO_x concentration is increased by 0.2ppbv~1ppbv over eastern China and the West Pacific. The elevation of NO_x concentration should be attributed to the depletion of O_3 and the conversion of gas-phase HNO_3 back to NO_x (Yarwood et al., 2005). As a result of excessive SO_4^{2-} production from dust chemistry, concentration of NO_3^- is decreased under the Dust_Chem scenario due to the thermal-dynamic equilibrium between $SO_4^{2-} - NH_4^+ - NO_3^-$. The equilibrium drives the inorganic aerosols to convert from NH_4NO_3 to $(NH_4)_2SO_4$ over eastern China with intensive anthropogenic SO_2 and NO_x emissions from industry and power sectors, but insufficient NH_3 to neutralize all the acid anions. On the other hand, over the western Pacific and Japan, where SO_2 and NO_x emissions are less intensive, concentration of NO_3^- is increased slightly due to the productions indicated by reactions R8 and R10. Consequently, over eastern and central China, removed NO_3^- evaporate back to HNO_3, which again push the gas-phase equilibrium towards production of NO_x, and thus leads to the increase of NO_x but decrease of HNO_3 and NO_3^-. Meanwhile, with the upper

limit of uptake coefficients, the production rate of HNO_3 catches up with the removal rate of NO_3^-, which helps to slow down the decrease of NO_3^- over China and accelerate the increase of NO_3^- over the western Pacific and Japan. Our result is consistent with the findings from other studies. Wang et al. (2012) also reported the increase of NO_x and decrease of HNO_3 and NO_3^- concentrations due to dust chemistry over East Asia. Li et al. (2012) report that NO_3^- concentration with lower uptake coefficient is about 5μg/m^3 (30%) lower than the base case simulation (with "best guess" uptake coefficient suggested in Zhu et al. (2010)), and NO_3^- predicted by high uptake coefficient is about 12μg/m^3 (100%) higher than the base case at Shanghai and Xiamen.

The impact of dust chemistry shown in Figure 6 suggests comparable results as other modeling assessments, but very few previous studies incorporated observation data to validate further the impact indicated by the model. To evaluate the model's capability of representing dust chemistry and also determine the best fit uptake coefficients, observations from EANET are used to compare with simulations from Dust_Profile, Dust_Chem, and Dust_ChemHigh. Evaluation statistics are summarized in Table 6. Simulation results from different scenarios for O_3 all agree well with observations as indicated by the statistics. O_3 is overpredicted by 1.26% without dust chemistry in the CMAQ, and underpredicted by -1.97% and -4.43% with lower and upper uptake coefficients, respectively. SO_2 is overpredicted in all scenarios, but the NMB value is reduced from 90.7% without dust chemistry to 69.8% and 63.7% with lower and upper uptake coefficients, respectively. Evaluation statistics for HNO_3 and NO_x show a similar response as SO_2, where heterogeneous chemistry helps to reduce the large overestimations from 109.03% without dust chemistry to 85.17% and 81.24% with lower and upper limits of uptake coefficients, respectively. The positive bias for SO_2 and HNO_3 should be attributed to the overestimated anthropogenic emissions (Dong and Fu, 2015a; Wang et al., 2011). For NO_x evaluation, however, model overestimation is increased from 35.61% under the Dust_Profile scenario to 37.79% and 38.21% under the Dust_Chem and Dust_ChemHigh scenarios, respectively. Overestimation of NO_x emission should be responsible for the positive bias from the CMAQ as indicated by previous studies (Dong and Fu, 2015a), but implementing dust chemistry into the model leads to larger overprediction of NO_x. Concentration of SO_4^{2-} is underpredicted by 16.28% without dust chemistry, yet the simulation overpredicts SO_4^{2-}

by 13.74% and 29.43% under Dust_Chem and Dust_ChemHigh scenarios, respectively. For NO_3^- predictions, dust chemistry helps to reduce the underprediction from 13.07% under the Dust_Profile scenario to -1.97% under Dust_Chem scenario. But the simulation is boosted up too much with upper limit of coefficients and it overpredicts NO_3^- concentration by 24.09% under the Dust_ChemHigh scenario. Note that EANET data are collected from Japanese sites so that Dust_Chem and Dust_ChemHigh show consistent increases of NO_3^-, as shown in Figure 6. Statistics shown in Table 6 suggest that implementing heterogeneous chemistry seems able to improve the CMAQ performance for most of the species except O_3 and NO_x, but the lower limit of uptake coefficients favors prediction of SO_4^{2-} and NO_3^-, and the upper limit of uptake coefficients has a better prediction for SO_4^{2-} and HNO_3. Although these statistics show competitive performance between Dust_Chem and Dust_ChemHigh, the lower limit of the uptake coefficient might be more appropriate if we consider the uncertainty within the baseline anthropogenic emissions. With both surface observations and satellite retrievals, Dong and Fu (2015a) demonstrated that the CMAQ overpredicted NO_x and SO_2 over East Asia between 2006 and 2010 by around 30% and 20%, respectively, due to overestimation in anthropogenic emissions. Wang et al. (2011) also report overestimation of SO_2 by 14% over China. Implementing dust chemistry helps to reduce simulated concentrations of SO_2, NO_x, and HNO_3, so it can balance part of the positive bias caused by anthropogenic emissions, but the statistics for SO_4^{2-} and NO_3^- indicate that the counter effect caused by using the upper limit of uptake coefficients might be too excessive and push the balance towards overestimation of aerosols as a side effect. Consequently, without explicitly excluding the bias within anthropogenic emissions, no solid conclusion could be achieved regarding the preference of uptake coefficients.

4. Discussion

4.1 Simulating a severe dust storm event

In this section we probe in to the capability of the CMAQ for reproducing a severe dust event. Many studies have reported that spring 2010 had the most severe dust storms in recent decades (Bian et al., 2011; Li et al., 2012) due to nation-wide drought in China.

PM_{10} observations were more than 1,000μg/m^3 at Beijing (Han et al., 2012), 1,600μg/m^3 at Seoul (Tatarov et al., 2012), and 1,200μg/m^3 at Taiwan (Tsai et al., 2013). These studies mainly focused on the impact of dust storms on a local scale, and the understanding about the emission and transport of the dust event on a regional scale is not well-developed. Here we examined this severe dust event with model simulations, satellite observations, and also surface measurements from multiple networks. Figure 7 displays the MODIS AOD and simulated AOD from the CMAQ Dust_Chem scenario during the severe dust storm episode from 19 to 21 March 2010. Simulated AOD is derived by following the approach described in Huang et al. (2013) for 11:00AM local time only to accommodate with the nadir view time by the MODIS. Spatial distributions of satellite agree well with the simulation on a daily scale, indicating that the model can generally reproduce the column density and long-range transport of dust particles. As shown in Figure 7 (b), the CMAQ simulation suggests that a large amount of dust emissions were uplifted on March 19th from the Gobi and increased AOD values over the desert and northern China. The heavy dust emission on 19 March had been identified with OMI by Li et al. (2011), Figure 8 (a) also indicates consistently high AOD values around northern China. As the dust plume moved eastwards, both the MODIS and the CMAQ suggests that AOD in the eastern coastal area of China increased from about 0.8 on March 19th to more than 2.0 on March 20th. On March 21st, the majority of the dust plume was pushed eastward and started to build up AOD over the west Pacific and Japan.

To further examine the dust event, forward trajectory is analyzed to characterize the transport pathway of dust plumes with the Hybrid Single-Particle Lagrangian Integrated Trajectory (HYSPLIT) model from NOAA/Air Resources Laboratory (Draxler and Rolph, 2015; Rolph 2015). Movement of air mass was analyzed for 72 hours, starting from 0:00 UTC (8:00 local time) on March 19th, 2010 at the Gobi, with the forward trajectories shown in Figure 8(f). Air masses at 500 (red line), 1,000 (blue line), and 2,000 meters (green line) moved southeastward until March 20th, when the higher plume turned east and moved across Japan and the west Pacific, while the lower plumes continued towards the eastern coastal area of China and finally reached Taiwan on March 21st. The HYSPLIT trajectory showed consistent transport of dust plumes as the MODIS and the CMAQ AOD analysis.

To understand the impact of dust storms along the transport pathway, we compare the simulated and observed surface level PM_{10} on a daily scale for all of March 2010 at selected stations along the transport pathway, as indicated by Figure 8(f). Simulations from the Dust_Chem (black lines in Figs. 8(a)-(e) and (g)-(o)) and the Dust_Off scenarios (blue lines in Fig. 8(a)-(e) and (g)-(o)) are analyzed to examine the model performance. Temporal variations of PM_{10} with observations from the API (red circles) are examined at Beijing, Lanzhou, Nanjing, Fuzhou, Lianyungang, and Shanghai as shown in Figures 8(a), (b), (c), (d), (e), and (k), respectively. Observed PM_{10} concentrations increased rapidly from less than 300μg/m^3 on 18 March to more than 600μg/m^3 at Beijing and 480μg/m^3 at Lianyungang on 19 March. In central and eastern China, concentrations of PM_{10} peaked on 21 March at Nanjing and Shanghai, and the API reached the measurement ceiling value of 600μg/m^3. In southern China, PM_{10} was also elevated to 600μg/m^3 at Xiamen on 22 March. Temporal variation in these cities suggested that PM_{10} concentrations were elevated with the onset of the dust storm, which moved from the Gobi to southeastern China from 19 to 21 March. PM_{10} concentrations fell back under 300μg/m^3 after the event. Lanzhou reached a peak of PM_{10} concentration as 500μg/m^3 on 14 March, which should be attributed to the impact of the dust storm that originated from the Taklamakan. Ling et al. (2011) also reported an observed 507μg/m^3 PM_{10} on 14 March at Lanzhou. Observations from EANET and the TAQMN are also employed to examine the long-range transport of dust over the West Pacific and Taiwan. Temporal variations of PM_{10} at three EANET sites (green diamonds) including Oki, Ogasawara, and Hedo are shown in Figures 8(h), (i), and (j), respectively. PM_{10} concentrations at these sites all showed consistent increase with the onset of dust on 21 or 22 March. At Xinzhuang, as shown in Figure 8(g), observations from the TAQMN (purple circles) demonstrated that local PM_{10} was increased from less than 100μg/m^3 on 20 March to more than 700μg/m^3 on 21 March due to the impact of the dust storm. Simulated PM_{10} from the Dust_Chem scenario agreed well with observations from different networks all over the domain. Predictions from the Dust_Chem and Dust_Off scenarios were almost the same at all stations during the non-dust period from 1 to 10 March, yet the Dust_Chem scenario was able to reproduce the rapid elevation of PM_{10} during the dust event. However, noticeable discrepancy was also found between the Dust_Chem prediction and observations. In general, the CMAQ overpredicted PM_{10}

slightly during the dust event at most of the API sites in China, but failed to reproduce the high concentrations at Lanzhou before 15 March and after 20 March. To help understand the model performance of predicting fine particles from dust, daily variations of AOD from the AERONET observations and the CMAQ simulations are also examined at four stations, including Beijing, the Semi-Arid Climate Observatory Laboratory (SACOL) station at Lanzhou (Ling et al., 2011), Osaka, and EPA-NCU (Taiwan Environment Protection Agency station at National Central University), as show in Figures 9 (l), (m), (n), and (o), respectively. Temporal variations of AOD were consistent with the daily changes of PM_{10} at these cities along the dust plume movement trajectory. The highest AOD was found on 14 March at the SACOL station, which was consistent with the rapid increase of PM_{10} concentrations at Lanzhou. Moderate underestimations of AOD were also found at Lanzhou and EPA-NCU stations during the dust events, indicating that fine mode aerosols were also underestimated over this region. In general, comparisons between the CMAQ and observations from MODIS and surface networks suggest that the model is capable of reproducing the severe dust storm event in terms of spatial distribution, transport, and concentration of dust particles, with possible underestimation of dust emission from the Taklamakan.

4.2 Remaining uncertainties within the modeling system

Despite the improvements of model performance demonstrated in the previous sections, it is necessary to note that there are some important remaining uncertainties within the modeling system. The first type of uncertainty is related to the anthropogenic emissions. Assessment of dust prediction capability of the model was primarily performed by comparing the simulation with observations, yet the bias caused by anthropogenic emissions would affect the bias from the dust prediction. So it is difficult to distinguish the uncertainties that arise from dust treatment in the model. Figure 9 displays the dust emission rate (Tg/day) from the Dust_Chem scenario (blue rectangles, with blue dash line indicating the trend), simulation bias of PM_{10} at the API stations (red circles, with red dash line indicating the trend), and simulation bias of PM_{10} at EANET stations (green diamonds, with green dash line indicating the trend) with all variables averaged on a monthly scale. Prediction from the CMAQ suggests a slightly increasing trend of dust emission from 2006 to 2010, which is consistent with the decadal increase of dust reported by Kurosaki et al.

(2011) due to changes of soil erodibility over Mongolia and northeastern China. Simulation biases of PM_{10} agree fairly well with the dust emission at both the API and EANET stations, indicating that overall underprediction of PM_{10} over East Asia has a smaller discrepancy for years with stronger dust events. Assuming there is persistent underestimation of primary PM emissions in the anthropogenic inventory, more dust emissions will apparently help to reduce the modeling bias for total PM_{10}. This is also consistent with previous studies (Wang et al., 2011; Dong and Fu. 2015a) which reported a systematic underestimation of anthropogenic emission of primary particles over China.

The second type of uncertainty lies within the friction velocity threshold u_{*_t}, which is affected by soil moisture fraction that might be overestimated by the WRF. Although in this study the simulation performance is improved with the initial threshold friction velocity constants u_{*_c} adjusted by avoiding the double counting of soil moisture effect, there are still non-negligible biases as shown in Section 3. Both the five-year average modeling bias shown in Figure 3(d) and temporal variations shown in Figure 8 suggest possible overestimated dust emission from the Gobi and underestimated dust from the Taklamakan. The averaged u_{*_t} calculated by the CMAQ is 0.19m/s and 0.14m/s over the Taklamakan and Gobi, respectively, with the soil moisture factor f_{soilm} as 1.21 and 1.13, respectively, indicating that the Taklamakan needs higher friction velocity in order to generate dust because of the more significant soil moisture impact than the Gobi. However, some recent field measurement studies suggest that the u_{*_t} in the Taklamakan is lower than that over the Gobi. He et al. (2010) conducted measurements at three sites inside the Taklamakan and reported the value of u_{*_t} as 0.25m/s, 0.27m/s, and 0.21m/s at three different sites, and Yang et al. (2011) also reported the value of u_{*_t} as 0.24 m/s at Tazhong (~39.03°N, 83.65°E). For the Gobi, Li and Zhang (2011) reported the value of u_{*_t} as 0.34 m/s ~0.42 m/s based on measurements made in April 2006 and 2008. Field measurements defined u_{*_t} as equal to the value of friction velocity u_* when dust concentration is increased by 20% for at least one-half hour (Li and Zhang, 2011), thus the reported values of u_{*_t} from the measurement studies are higher than the calculations from the model. But

the comparison between the Taklamakan and Gobi measurements suggests that the model may either underestimate at the Gobi or overestimate at the Taklamakan for u_{*_t}. Since f_{soilm} is determined by soil moisture fraction, we compare the soil moisture from FNL (NCEP final analysis data) which is used to drive WRF in this study with another reanalysis dataset GLDAS (Global Land Data Assimilation System; (Rodell et al., 2004)). Figure 10 demonstrates the five-year averages (for March and April) of soil moisture fraction at top 10cm depth from (a) FNL and (b) GLDAS. Soil moisture is estimated to be 10~15% by FNL at both deserts, while the values from GLDAS are less than 5% at the Taklamakan and 5%~10% at the Gobi. Zender et al. (2003) reported that soil moisture from NCEP is too high over active dust emission areas and leads to negative AOD bias of the model on a global scale. With the WRF-NMMB/BSC-Dust model, Haustein et al. (2012) conducted simulations with meteorology driven by FNL and GLDAS respectively over north Africa and reported that the predictions with GLDAS had better agreement with the AERONET's AOD observations due to smaller friction velocity and slightly faster surface wind speed due to lower values of soil moisture. But no such sensitivity studies have been made over East Asia, and unfortunately there is no publicly available observation data for the period of 2006-2010 to examine the potential overestimation of soil moisture by FNL in our modeling domain. Although we previously reported consistent negative bias of surface temperature at 2 meters height for 2006-2010, which might be due to excessive soil moisture (Dong and Fu, 2015), more research efforts are required to verify the uncertainties caused by using FNL soil data.

The last type of uncertainty lies within the mass contribution of fine aerosols within dust emission. Elevated dust particles are distributed into fine and coarse mode aerosols with mass ratios of 0.2 and 0.8, respectively, in the CMAQ dust scheme. In this study however, the ratio of $PM_{2.5}$/TSP derived from observations at Duolun and Yulin are 0.42 and 0.39, respectively, indicating that fine particles should have higher mass contribution within East Asian dust. The data from Huang et al. (2010) indicated that the ratio of $PM_{2.5}$/TSP at Tazhong was 0.45 in spring 2007, which suggested an even higher fine particle mass contribution at the Taklamakan. Model evaluation results shown in Figure 5 also

demonstrate the systematic underestimations of both trace metals and total $PM_{2.5}$ concentrations at both dust source regions and downwind areas, while the concentrations of PM_{10} are slightly overestimated near the source region as demonstrated in Figure 3. Consequently, it is highly possible that the ratio of fine particles within dust emission should be higher. But since TSP also include all large particles >10μm, observations of both $PM_{2.5}$ and PM_{10} at active dust regions are urgently needed to help clearly characterize the ratio in the model.

5. Summary

Dust module development has been implemented into the CMAQ in this study. The initial threshold friction velocity constants are revised by removing the double counting of soil moisture in the default parameters; two source-dependent speciation profiles are derived based on local observations of dust emission from the Taklamakan and Gobi deserts; and dust heterogeneous chemistry is implemented. The CMAQ with its revised dust scheme is applied over East Asia for March and April from 2006 to 2010. Based on model evaluations with observation data from both ground-surface networks and satellite retrievals, the revised dust scheme is demonstrated to improve the model performance. Evaluation statistics suggest that NMB for PM_{10} simulation is reduced from -55% by default model to -16% by the revised model, and NMB for AOD is reduced from -31% to -22%. Applying source-dependent speciation profiles improves the simulation of trace metals. Heterogeneous chemistry with lower and upper limits of uptake coefficients is also investigated. Although simulations with dust chemistry are demonstrated to agree with observations better than those without chemistry for most of the pollutants, no solid conclusion could be made regarding the preference of uptake coefficients without explicitly excluding the uncertainty caused by anthropogenic emission. This is because simulation with lower coefficients has better agreement with observations for O_3, SO_4^{2-}, and NO_3^-, while simulation with upper coefficients has better performance for SO_2 and NO_2.

A severe dust storm episode from 19 to 21 March 2010 is investigated to examine the model performance during extreme dust event. The revised CMAQ modeling system successfully reproduces most of the PM_{10} and AOD observations in both near source

(China) and downwind areas (Japan and Taiwan). But some notable discrepancies are also found, indicating the slight overestimation of dust from the Gobi and underestimation of dust from the Taklamakan. Comparison of the FNL and GLDAS soil moisture fractions indicates that the excessive soil moisture within FNL might be responsible for the higher friction velocity threshold and lower dust emissions calculated by the CMAQ over the Taklamakan. But more sensitive studies with different reanalysis data inputs for WRF and the local soil moisture measurements in the deserts are needed to reach a solid conclusion. In addition, potential uncertainty is also identified within the mass contributions of fine and coarse mode particles from dust emission. Evaluation results indicate consistent underestimation of trace metals and $PM_{2.5}$ by 30%~50% at Duolun and Yulin close to the Gobi desert, yet the PM_{10} are generally overestimated slightly at adjacent cities. While measurements from Huang et al. (2010) suggested mass contribution as ~40% of fine particles in TSP, the value of 20% used in the current CMAQ might be too low for dust emissions from the Gobi and Taklamakan. In summary, the model development employed in this study has been demonstrated to enhance the capability of the CMAQ for simulating dust over East Asia regarding the chemical and physical processes involved, which can serve as a useful tool for further investigating the impacts of dust on regional climate over East Asia and elsewhere.

6. Acknowledgements

We thank NASA GSFC (Grant No. NNX09AG75G) and the National Natural Science Foundation of China (Grant No. 41429501) for their funding support. D. Tong is also particularly grateful for his award of a NASA ROSES grant (NNX13AO45G). We would like to acknowledge Edward J. Hyer for providing biomass burning emission, and we thank Dr. Keiichi Sato and Dr. Ayako Aoyagi from the Asia Center for Air Pollution Research for providing the EANET data. We would like to acknowledge Dr. George Lin of the National Center University for providing the AOD observations from Taiwan, and we would also like to acknowledge China MEP and Taiwan EPA for providing the observation data, and thank NASA for providing the AERONET and MODIS data. We thank the

National Institute for Computational Sciences (NICS) for providing the computer sources for the model simulations used in this research.

References

Appel, K. W., Pouliot, G. A., Simon, H., Sarwar, G., Pye, H. O. T., Napelenok, S. L., Akhtar, F., and Roselle, S. J.: Evaluation of dust and trace metal estimates from the Community Multiscale Air Quality (CMAQ) model version 5.0, Geoscientific Model Development, 6, 883-899, 2013.

Arimoto, R., Kim, Y. J., Kim, Y. P., Quinn, P. K., Bates, T. S., Anderson, T. L., Gong, S., Uno, I., Chin, M., Huebert, B. J., Clarke, A. D., Shinozuka, Y., Weber, R. J., Anderson, J. R., Guazzotti, S. A., Sullivan, R. C., Sodeman, D. A., Prather, K. A., and Sokolik, I. N.: Characterization of Asian Dust during ACE-Asia, Global and Planetary Change, 52, 23-56, 2006.

Bauer, S. E., Balkanski, Y., Schulz, M., Hauglustaine, D. A., and Dentener, F.: Global modeling of heterogeneous chemistry on mineral aerosol surfaces: Influence on tropospheric ozone chemistry and comparison to observations, Journal of Geophysical Research-Atmospheres, 109, D02304, DOI: 10.1029/2003JD003868 2004.Bian, H., Tie, X. X., Cao, J. J., Ying, Z. M., Han, S. Q., and Xue, Y.: Analysis of a Severe Dust Storm Event over China: Application of the WRF-Dust Model, Aerosol and Air Quality Research, 11, 419-428, 2011.

Bian, H. S., and Zender, C. S.: Mineral dust and global tropospheric chemistry: Relative roles of photolysis and heterogeneous uptake, Journal of Geophysical Research-Atmospheres, 108, 4672, doi:10.1029/2002JD003143, 2003.

Blanco, A., De Tomasi, F., Filippo, E., Manno, D., Perrone, M. R., Serra, A., Tafuro, A. M., and Tepore, A.: Characterization of African dust over southern Italy, Atmospheric Chemistry and Physics, 3, 2147-2159, 2003.

Carmichael, G. R., Tang, Y., Kurata, G., Uno, I., Streets, D., Woo, J. H., Huang, H., Yienger, J., Lefer, B., Shetter, R., Blake, D., Atlas, E., Fried, A., Apel, E., Eisele, F., Cantrell, C., Avery, M., Barrick, J., Sachse, G., Brune, W., Sandholm, S., Kondo, Y., Singh, H., Talbot, R., Bandy, A., Thorton, D., Clarke, A., and Heikes, B.: Regional-scale chemical transport modeling in support of the

analysis of observations obtained during the TRACE-P experiment, Journal of Geophysical Research-Atmospheres, 108, 8823, doi:10.1029/2002JD003117, 2003.

Chen, S. Y., Huang, J. P., Zhao, C., Qian, Y., Leung, L. R., and Yang, B.: Modeling the transport and radiative forcing of Taklimakan dust over the Tibetan Plateau: A case study in the summer of 2006, Journal of Geophysical Research-Atmospheres, 118, 797-812, 2013.

Chun, Y. S., Boo, K. O., Kim, J., Park, S. U., and Lee, M.: Synopsis, transport, and physical characteristics of Asian dust in Korea, Journal of Geophysical Research-Atmospheres, 106, 18461-18469, 2001.

Cwiertny, D. M., Young, M. A., and Grassian, V. H.: Chemistry and photochemistry of mineral dust aerosol, Annual Review of Physical Chemistry, 59, 27-51, 2008.

Darmenova, K. and Sokolik, I.N.: Dust emission and deposition in regional models, Third International Dust Workshop, Leipzig, Germany, September, (September 15, 01-03) 2008

Davis, J. M., Bhave, P. V., and Foley, K. M.: Parameterization of N2O5 reaction probabilities on the surface of particles containing ammonium, sulfate, and nitrate, Atmospheric Chemistry and Physics, 8, 5295-5311, 2008.

De Longueville, F., Hountondji, Y. C., Henry, S., and Ozer, P.: What do we know about effects of desert dust on air quality and human health in West Africa compared to other regions? Science of the Total Environment, 409, 1-8, 2010.

Dentener, F. J., Carmichael, G. R., Zhang, Y., Lelieveld, J., and Crutzen, P. J.: Role of mineral aerosol as a reactive surface in the global troposphere, Journal of Geophysical Research-Atmospheres, 101, 22869-22889, 1996.

Dong, X. Y., Li, J., Fu, J. S., Gao, Y., Huang, K., and Zhuang, G. S.: Inorganic aerosols responses to emission changes in Yangtze River Delta, China, Science of the Total Environment, 481, 522-532, 2014.

Dong, X. Y., and Fu, J. S.: Understanding interannual variations of biomass burning from Peninsular Southeast Asia, part I: Model evaluation and analysis of systematic bias, Atmospheric Environment, 116, 293-307, 2015a.

Dong, X. Y., and Fu, J. S.: Understanding interannual variations of biomass burning from Peninsular Southeast Asia, part II: Variability and different influences in lower and higher atmosphere levels, Atmospheric Environment, 115, 9-18, 2015b.

Draxler, R.R. and Rolph, G.D.: HYSPLIT (HYbrid Single-Particle Lagrangian Integrated Trajectory) Model access via NOAA ARL READY Website

(http://ready.arl.noaa.gov/HYSPLIT.php). August 1st, 2015, NOAA Air Resources Laboratory, Silver Spring, MD, 2015

EANET: EANET Data Report 2006, Acid Deposition Monitoring Network in East Aisa (EANET), 2007.

Engelstaedter, S., Kohfeld, K. E., Tegen, I., and Harrison, S. P.: Controls of dust emissions by vegetation and topographic depressions: An evaluation using dust storm frequency data, Geophysical Research Letters, 30, 1294, doi:10.1029/2002GL016471, 2003.

Fairlie, T. D., Jacob, D. J., Dibb, J. E., Alexander, B., Avery, M. A., van Donkelaar, A., and Zhang, L.: Impact of mineral dust on nitrate, sulfate, and ozone in transpacific Asian pollution plumes, Atmospheric Chemistry and Physics, 10, 3999-4012, 2010.

F´ecan, F., Marticorena, B., and Bergametti, G.: Parametrization of the increase of the aeolian erosion threshold wind friction velocity due to soil moisture for arid and semi-arid areas, Ann. Geophys., 17, 149–157, 1999.

Formenti, P., Elbert, W., Maenhaut, W., Haywood, J., and Andreae, M. O.: Chemical composition of mineral dust aerosol during the Saharan Dust Experiment (SHADE) airborne campaign in the Cape Verde region, September 2000, Journal of Geophysical Research-Atmospheres, 108, 8576, doi:10.1029/2002JD002648, 2003.

Forster, P., Ramaswamy, V., Artaxo, P., Berntsen, T., Betts, R., Fahey, D. W., Haywood, J., Lean, J., Lowe, D. C., Myhre, G., Nganga, J., Prinn, R., Raga, G., Schulz, M., and Van Dorland, R.: Radiative Forcing of Climate Change, in Climate Change 2007: The Physical Science Basis. Contribution of Working Group I to the Fourth Assessment Report of the Intergovernmental Panel on Climate Change, edited by S. Solomon, D. Qin, M. Manning, Z. Chen, M. Marquis, K. B. Averyt, M. Tignor,

and H. L. Miller, pp. 129–234, Cambridge Univ. Press, Cambridge, United Kingdom and New York, NY, USA, 2007.

Fu, X., Wang, S.X., Cheng, Z., Xing, J., Zhao, B., Wang, J.D., and Hao, J.M.: Source, transport and impacts of a heavy dust event in the Yangtze River Delta, China, in 2011. Atmospheric Chemistry and Physics, 14(3) 1239-1254, 2014

Gillette, D.A., Adams, J., Endo, A., Smith, D., and Kihl, R.: Threshold Velocities for Input of Soil Particles into the Air by Desert Soils. Journal of Geophysical Research-Oceans and Atmospheres, 85(Nc10) 5621-5630, 1980.

Gillette, D. A., Adams, J., Muhs, D., and Kihl, R.: Threshold friction velocities and rupture moduli for crusted desert soils for the input of soil particles into the air, Journal of Geophysical Research, 87**, 9003– 9015, 1982.**

Ginoux, P., Chin, M., Tegen, I., Prospero, J. M., Holben, B., Dubovik, O., and Lin, S. J.: Sources and distributions of dust aerosols simulated with the GOCART model, Journal of Geophysical Research-Atmospheres, 106, 20255-20273, 2001.

Grell, G. A., Peckham, S. E., Schmitz, R., McKeen, S. A., Frost, G., Skamarock, W. C., and Eder, B.: Fully coupled "online" chemistry within the WRF model, Atmospheric Environment, 39, 6957-6975, 2005.

Guenther, A., Karl, T., Harley, P., Wiedinmyer, C., Palmer, P. I., and Geron, C.: Estimates of global terrestrial isoprene emissions using MEGAN (Model of Emissions of Gases and Aerosols from Nature), Atmospheric Chemistry and Physics, 6, 3181-3210, 2006.

Han, X., Ge, C., Tao, J. H., Zhang, M. G., and Zhang, R. J.: Air Quality Modeling for a Strong Dust Event in East Asia in March 2010, Aerosol and Air Quality Research, 12, 615-628, 2012.

Haustein, K., Perez, C., Baldasano, J. M., Jorba, O., Basart, S., Miller, R. L., Janjic, Z., Black, T., Nickovic, S., Todd, M. C., Washington, R., Muller, D., Tesche, M., Weinzierl, B., Esselborn, M., and Schladitz, A.: Atmospheric dust modeling from meso to global scales with the online NMMB/BSC-Dust model - Part 2: Experimental campaigns in Northern Africa, Atmospheric Chemistry and Physics, 12, 2933-2958, 2012.

Heikes, B. G., and Thompson, A. M.: Effects of Heterogeneous Processes on No3, Hono, and Hno3 Chemistry in the Troposphere, Journal of Geophysical Research-Oceans and Atmospheres, 88, 883-895, 1983.

Huang, K., Zhuang, G. S., Li, J. A., Wang, Q. Z., Sun, Y. L., Lin, Y. F., and Fu, J. S.: Mixing of Asian dust with pollution aerosol and the transformation of aerosol components during the dust storm over China in spring 2007, Journal of Geophysical Research-Atmospheres, 115, D00K13, doi:10.1029/2009JD013145, 2010.

Huang, K., Fu, J. S., Hsu, N. C., Gao, Y., Dong, X., Tsay, S.-C., and Lam, Y. F.: Impact assessment of biomass burning on air quality in Southeast and East Asia during BASE-ASIA, Atmospheric Environment, 78, 291–302, doi:10.1016/j.atmosenv.2012.03.048, 2013.

Huneeus, N., et al.: Global dust model intercomparison in AeroCom phase I, Atmospheric Chemistry and Physics, 11(15), 7781–7816, 2011.

Kandler, K., Benker, N., Bundke, U., Cuevas, E., Ebert, M., Knippertz, P., Rodriguez, S., Schutz, L., and Weinbruch, S.: Chemical composition and complex refractive index of Saharan Mineral Dust at

Izana, Tenerife (Spain) derived by electron microscopy, Atmospheric Environment, 41, 8058-8074, 2007.

Krueger, B. J., Grassian, V. H., Cowin, J. P., and Laskin, A.: Heterogeneous chemistry of individual mineral dust particles from different dust source regions: The importance of particle mineralogy, Atmospheric Environment, 38, 6253-6261, 2004.

Kumar, R., Barth, M. C., Pfister, G. G., Naja, M., and Brasseur, G. P.: WRF-Chem simulations of a typical pre-monsoon dust storm in northern India: Influences on aerosol optical properties and radiation budget, Atmospheric Chemistry and Physics, 14, 2431-2446, 2014.

Kurosaki, Y., and Mikami, M.: Regional difference in the characteristic of dust event in East Asia: Relationship among dust outbreak, surface wind, and land surface condition, Journal of the Meteorological Society of Japan, 83A, 1-18, 2005.

Lam, Y. F., and Fu, J. S.: A novel downscaling technique for the linkage of global and regional air quality modeling, Atmospheric Chemistry and Physics, 9, 9169-9185, 2009.

Li, J., Wang, Z. F., Zhuang, G., Luo, G., Sun, Y., and Wang, Q.: Mixing of Asian mineral dust with anthropogenic pollutants over East Asia: A model case study of a super-duststorm in March 2010, Atmospheric Chemistry and Physics, 12, 7591-7607, 2012.

Li, J. W., Han, Z. W., and Zhang, R. J.: Model study of atmospheric particulates during dust storm period in March 2010 over East Asia, Atmospheric Environment, 45, 3954–3964, doi:10.1016/j.atmosenv.2011.04.068, 2011.

Li, W. Y., Shen, Z. B, Lu, S. H., and Li, Y. H: Sensitivity Tests of Factors Influencing Wind Erosion, Journal of Desert Research, 27, 984–993, 2007.

Li, X. and Zhang, H. S.: Research on threshold friction velocities during dust events over the Gobi Desert in northwest China, Journal of Geophysical Research, 116, D20210, doi:10.1029/2010JD015572, 2011.

Liao, H., Seinfeld, J. H., Adams, P. J., and Mickley, L. J.: Global radiative forcing of coupled tropospheric ozone and aerosols in a unified general circulation model, Journal of Geophysical Research-Atmospheres, 109, D16207, doi:10.1029/2003JD004456, 2004.

Ling, X., Guo, W., Zhao, Q., and Zhang, B.: A case study of a typical dust storm event over the Loess Plateau of northwest China Atmos. Ocean. Sci. Lett., 4 (6), 344–348, 2011.

Liu, M., and Westphal, D. L.: A study of the sensitivity of simulated mineral dust production to model resolution, Journal of Geophysical Research-Atmospheres, 106, 18099-18112, 2001.

Ma, C. J., Kasahara, M., Holler, R., and Kamiya, T.: Characteristics of single particles sampled in Japan during the Asian dust-storm period, Atmospheric Environment, 35, 2707-2714, 2001.

Marticorena, B., Bergametti, G., Aumont, B., Callot, Y., NDoume, C., and Legrand, M.: Modeling the atmospheric dust cycle .2. Simulation of Saharan dust sources. Journal of Geophysical Research-Atmospheres, 102(D4) 4387-4404, 1997.

Matsuki, A., Iwasaka, Y., Shi, G. Y., Zhang, D. Z., Trochkine, D., Yamada, M., Kim, Y. S., Chen, B., Nagatani, T., Miyazawa, T., Nagatani, M., and Nakata, H.: Morphological and chemical modification

of mineral dust: Observational insight into the heterogeneous uptake of acidic gases, Geophysical Research Letters, 32, L22806, doi:10.1029/2005GL024176, 2005.

Miller, R. L., Cakmur, R. V., Perlwitz, J., Geogdzhayev, I. V., Ginoux, P., Koch, D., Kohfeld, K. E., Prigent, C., Ruedy, R., Schmidt, G. A., and Tegen, I.: Mineral dust aerosols in the NASA goddard institute for Space Sciences ModelE atmospheric general circulation model, Journal of Geophysical Research-Atmospheres, 111, D06208, doi:10.1029/2005JD005796, 2006.

Muller, J. F., Stavrakou, T., Wallens, S., De Smedt, I., Van Roozendael, M., Potosnak, M. J., Rinne, J., Munger, B., Goldstein, A., and Guenther, A. B.: Global isoprene emissions estimated using MEGAN, ECMWF analyses and a detailed canopy environment model, Atmospheric Chemistry and Physics, 8, 1329-1341, 2008.

Owen, P.R.: Saltation of uniform grains in air. Journal of Fluid Mechanics, 20(2), 225-242, 1964

Park, S. U., and In, H. J.: Parameterization of dust emission for the simulation of the yellow sand (Asian dust) event observed in March 2002 in Korea, Journal of Geophysical Research-Atmospheres, 108, 4618, doi:10.1029/2003JD003484, 2003.

Pathak, R. K., Wang, T., and Wu, W. S.: Nighttime enhancement of PM2.5 nitrate in ammonia-poor atmospheric conditions in Beijing and Shanghai: Plausible contributions of heterogeneous hydrolysis of N2O5 and HNO3 partitioning, Atmospheric Environment, 45, 1183-1191, 2011.

Prospero, J. M.: Long-term measurements of the transport of African mineral dust to the southeastern United States: Implications for regional air quality, Journal of Geophysical Research-Atmospheres, 104, 15917-15927, 1999.

Pun, B. K., and Seigneur, C.: Sensitivity of particulate matter nitrate formation to precursor emissions in the California San Joaquin Valley, Environmental Science & Technology, 35, 2979-2987, 2001.

Qian, W. H., Quan, L. S., and Shi, S. Y.: Variations of the dust storm in China and its climatic control, Journal of Climate, 15, 1216-1229, 2002.

Reddy, M. S., Boucher, O., Balkanski, Y., and Schulz, M.: Aerosol optical depths and direct radiative perturbations by species and source type, Geophysical Research Letters, 32, L12803, doi:10.1029/2004GL02174, 2005.

Reid, E. A., Reid, J. S., Meier, M. M., Dunlap, M. R., Cliff, S. S., Broumas, A., Perry, K., and Maring, H.: Characterization of African dust transported to Puerto Rico by individual particle and size segregated bulk analysis, Journal of Geophysical Research-Atmospheres, 108, 8591, doi:10.1029/2002JD00293, 2003.

Reid, J. S., Hyer, E. J., Prins, E. M., Westphal, D. L., Zhang, J. L., Wang, J., Christopher, S. A., Curtis, C. A., Schmidt, C. C., Eleuterio, D. P., Richardson, K. A., and Hoffman, J. P.: Global Monitoring and Forecasting of Biomass-Burning Smoke: Description of and Lessons From the Fire Locating and Modeling of Burning Emissions (FLAMBE) Program, IEEE Journal of Selected Topics in Applied Earth Observations and Remote Sensing, 2, 144-162, 2009.

Rodell, M., Houser, P. R., Jambor, U., Gottschalck, J., Mitchell, K., Meng, C. J., Arsenault, K., Cosgrove, B., Radakovich, J., Bosilovich, M., Entin, J. K., Walker, J. P., Lohmann, D., and Toll, D.:

The global land data assimilation system, B Am Meteorol Soc, 85, 381-+, 10.1175/Bams-85-3-381, 2004.

Rosenfeld, D., Rudich, Y., and Lahav, R.: Desert dust suppressing precipitation: A possible desertification feedback loop, Proceedings of the National Academy of Sciences of the United States of America, 98, 5975-5980, 2001.

Rolph, G.D.: Real-time Environmental Applications and Display sYstem (READY) Website (http://ready.arl.noaa.gov), August 1st, 2015, NOAA Air Resources Laboratory, Silver Spring, MD, 2015

Sarwar, G., Roselle, S. J., Mathur, R., Appel, W., Dennis, R. L., and Vogel, B.: A comparison of CMAQ HONO predictions with observations from the northeast oxidant and particle study, Atmospheric Environment, 42, 5760-5770, 2008.

Shao, Y., and Dong, C. H.: A review on East Asian dust storm climate, modelling and monitoring, Global and Planetary Change, 52, 1-22, 2006.

Simon, H., Beck, L., Bhave, P.V., Divita, F., Hsu, Y., Luecken, D., Mobley, J.D., Pouliot, G.A., Reff, A., Sarwar, G., and Strum, M.: The development and uses of EPA's SPECIATE database. Atmospheric Pollution Research, 1(4) 196-206, 2010.

Skamarock, W.C., Klemp, J.B., Dudhia, J., Gill, D.O., Barker, D.M., Duda, M.G., Huang, X.Y., Wang, W., and Powers, J.G.: A Description of the Advanced Research WRF Version 3. NCAR, NCAR Technical Note NCAR/TN-475+STR, DOI: 10.5065/D68S4MVH, 2008.

Sun, Y. L., Zhuang, G. S., Wang, Y., Zhao, X. J., Li, J., Wang, Z. F., and An, Z. S.: Chemical composition of dust storms in Beijing and implications for the mixing of mineral aerosol with pollution aerosol on the pathway, Journal of Geophysical Research-Atmospheres, 110, D24209, doi:10.1029/2005JD006054, 2005.

Tang, Y. H., Carmichael, G. R., Kurata, G., Uno, I., Weber, R. J., Song, C. H., Guttikunda, S. K., Woo, J. H., Streets, D. G., Wei, C., Clarke, A. D., Huebert, B., and Anderson, T. L.: Impacts of dust on regional tropospheric chemistry during the ACE-Asia experiment: A model study with observations, Journal of Geophysical Research-Atmospheres, 109, D19S21, doi:10.1029/2003JD003806, 2004.

Tatarov, B., Muller, D., Noh, Y. M., Lee, K. H., Shin, D. H., Shin, S. K., Sugimoto, N., Seifert, P., and Kim, Y. J.: Record heavy mineral dust outbreaks over Korea in 2010: Two cases observed with

multiwavelength aerosol/depolarization/Raman-quartz lidar, Geophysical Research Letters, 39, L14801, doi:10.1029/2012GL051972, 2012.

Tsai, F. J., Fang, Y. S., and Huang, S. J.: Case Study of Asian Dust Event on March 19-25, 2010 and Its Impact on the Marginal Sea of China, Journal of Marine Science and Technology-Taiwan, 21, 353-360, 2013.

Tong, D. Q., Bowker, G. E., He, S., Byun, D. W., Mathur, R., and Gillette, D. A.: Development of a windblown dust emission model FENGSHAA description and initial application in the United States, In review, 2015.

Uno, I., Amano, H., Emori, S., Kinoshita, K., Matsui, I., and Sugimoto, N.: Trans-Pacific yellow sand transport observed in April 1998: A numerical simulation, Journal of Geophysical Research-Atmospheres, 106, 18331-18344, 2001.

Usher, C. R., Michel, A. E., and Grassian, V. H.: Reactions on mineral dust, Chemical Reviews, 103, 4883-4939, 2003.

Vogel, B., Vogel, H., Kleffmann, J., and Kurtenbach, R.: Measured and simulated vertical profiles of nitrous acid - Part II. Model simulations and indications for a photolytic source, Atmospheric Environment, 37, 2957-2966, 2003.

Wang, K., Zhang, Y., Nenes, A., and Fountoukis, C.: Implementation of dust emission and chemistry into the Community Multiscale Air Quality modeling system and initial application to an Asian dust storm episode, Atmospheric Chemistry and Physics, 12, 10209-10237, doi:10.5194/acp-12-10209-2012, 2012.

Wang, S. X., Xing, J., Chatani, S., Hao, J. M., Klimont, Z., Cofala, J., and Amann, M.: Verification of anthropogenic emissions of China by satellite and ground observations, Atmospheric Environment, 45, 6347-6358, 2011.

Washington, R., Todd, M., Middleton, N. J., and Goudie, A. S.: Dust-storm source areas determined by the total ozone monitoring spectrometer and surface observations, Annals of the Association of American Geographers, 93, 297-313, 2003.

Xing, J., Mathur, R., Pleim, J., Hogrefe, C., Gan, C.-M., Wong, D. C., Wei, C., Gilliam, R., and Pouliot, G.: Observations and modeling of air quality trends over 1990−2010 across the Northern Hemisphere: China, the United States and Europe. Atmospheric Chemistry and Physics, 15, 2723−2747, 2015.

Yarwood, J., Rao, S., Yocke, Ma., Whitten, G.Z., and Reyes, S.: Updates to the Carbon Bond Mechanism: CB05, Final Report to the US EPA, RT-0400675, Chapel Hill, NC, December, 2005.

Zhang, X. Y., Gong, S. L., Zhao, T. L., Arimoto, R., Wang, Y. Q., and Zhou, Z. J.: Sources of Asian dust and role of climate change versus desertification in Asian dust emission, Geophysical Research Letters, 30, 2272, doi:10.1029/2003GL018206, 2003.

Zhao, B., Wang, S. X., Dong, X. Y., Wang, J. D., Duan, L., Fu, X., Hao, J. M., and Fu, J.: Environmental effects of the recent emission changes in China: Implications for particulate matter pollution and soil acidification, Environmental Research Letters, 8, 024031, doi:10.1088/1748-9326/8/2/024031, 2013.

Zhao, C., Liu, X., Leung, L. R., Johnson, B., McFarlane, S. A., Gustafson, W. I., Fast, J. D., and Easter, R.: The spatial distribution of mineral dust and its shortwave radiative forcing over North

Africa: Modeling sensitivities to dust emissions and aerosol size treatments, Atmospheric Chemistry and Physics, 10, 8821-8838, 2010.

Zhu, H. and Zhang, H. S.: An estimation of the threshold friction velocities over the three different dust storm source areas in northwest China (in Chinese), Acta. Meteorol. Sin., 68, 977–984, 2010.

Zhuang, G. S., Yi, Z., Duce, R. A., and Brown, P. R.: Link between Iron and Sulfur Cycles Suggested by Detection of Fe(Ii) in Remote Marine Aerosols, Nature, 355, 537-539, 1992.

Table 1. Dust emission speciation profiles from the default CMAQ, and the profiles derived in this study for the Taklamakan and Gobi deserts. Simulation results of ACA, AMG, and AK (in bold) are evaluated against observations in this study.

Model Species	Description	Mass Contributions (%)					
		Fine Mode (I,J mode in CMAQ ≤2.5μm)			Coarse Mode (K mode in CMAQ ≤10 μm)		
		Default	Taklamakan	Gobi	Default	Taklamakan	Gobi
ASO4	Sulfate (SO_4^{2-})	2.5	3.554	0.953	2.655	2.825	0.471
ANO3	Nitrate (NO_3^-)	0.02	0.181	0.204	0.16	0.125	0.084
ACL	Chloride (Cl^-)	0.945	2.419	0.544	1.19	2.357	0.094
ANH4	Ammonium (NH_4^+)	0.005	0.098	0.346	0	0.066	0.185
ANA	Sodium (Na^+)	3.935	2.234	1.016	0	2.056	0.301
ACA	**Calcium (Ca_2^+)**	**7.94**	**2.063**	**1.788**	**0**	**1.423**	**1.082**
AMG	**Magnesium (Mg_2^+)**	**0**	**0.165**	**0.799**	**0**	**0.121**	**0.819**
AK	**Potassium (K^+)**	**3.77**	**0.153**	**0.282**	**0**	**0.108**	**0.121**
APOC	Primary Organic Carbon	1.075	1.075	1.075	0	0	0
APNCOM	Non-carbon organic matter	0.43	0.43	0.43	0	0	0
AEC	Elementary carbon	0	0	0	0	0	0
AFE	Iron (Fe)	3.355	4.689	2.425	0	3.75	3.055
AAL	Aluminum (Al)	5.695	5.926	4.265	0	4.987	4.641
ASI	Silicon (Si)	19.425	20.739	14.929	0	17.454	16.245
ATI	Titanium (Ti)	0.28	0.312	0.337	0	0.285	0.365
AMN	Manganese (Mn)	0.115	0.0758	0.063	0	0.062	0.072

AH2O	Water (H_2O)	0.541	0.541	0.541	0	0	0
AOTHR	Unspeciated	50.219	55.345	70.002	0	0	0
ASOIL	Non-anion dust	0	0	0	95.995	64.382	72.464

1
2

1 Table 2. Heterogeneous reactions and uptake coefficients

No.	Reaction	Uptake coefficient	References
Default heterogeneous reactions in CMAQv5.0.1			
C1	$N_2O_5 + H_2O \longrightarrow 2HNO_3$	$\gamma = \begin{cases} (x_1 + x_2) \times \gamma_d^* + x_3 \times \min(\gamma_d^*, \gamma_3), RH < CRH \\ \sum_{i=1}^{3} x_i \times \gamma_i^*, RH > IRH \\ 0.02, otherwise \end{cases}$ where x_1, x_2, x_3 and $\gamma_1, \gamma_2, \gamma_3$ are the normalized molar concentrations and N_2O_5 uptake coefficients on NH_4HSO_4, $(NH_4)_2SO_4$, and NH_4NO_3 respectively, $\gamma_d^* = \min(\gamma_d, 0.0124)$ where γ_d is the uptake coefficient on dry particles determined by relative humidity and temperature, RH is relative humidity, CRH is crystallization relative humidity, IRH is ice formation relative humidity determined by temperature	Davis et al. (2008)
C2	$2NO_2 + H_2O \longrightarrow HONO + HNO_3$	$K = 5.0 \times 10^{-6} \times A_p$	Vogel et al. (2003)
Implemented dust heterogeneous reactions in this work			
R1	$O_3 + dust \longrightarrow products$	$5.0 \times 10^{-5} \sim 1.0 \times 10^{-4}$	Zhu et al. (2010)
R2	$OH + dust \longrightarrow products$	$0.1 \sim 1.0$	Zhu et al. (2010)
R3	$H_2O_2 + dust \longrightarrow products$	$1.0 \times 10^{-4} \sim 2.0 \times 10^{-3}$	Zhu et al. (2010)
R4	$CH_3COOH + dust \longrightarrow products$	1.0×10^{-3}	Zhu et al. (2010)
R5	$CH_3OH + dust \longrightarrow products$	1.0×10^{-5}	Zhu et al. (2010)

R6	$CH_2O + dust \longrightarrow products$	1.0×10^{-5}	Zhu et al. (2010)
R7	$HNO_3 + dust \longrightarrow 0.5NO_3^- + 0.5NO_x$	$1.1\times10^{-3} \sim 0.2$	Dentener et al. (1996)
R8	$N_2O_5 + dust \longrightarrow 2NO_3^-$	$1\times10^{-3} \sim 0.1$	Zhu et al. (2010)
R9	$NO_2 + dust \longrightarrow NO_3^-$	$4.4\times10^{-5} \sim 2.0\times10^{-4}$	Underwood et al. (2001)
R10	$NO_3 + dust \longrightarrow NO_3^-$	$0.1 \sim 0.23$	Underwood et al. (2001)
R11	$NO_3 + dust \longrightarrow HNO_3$	1.0×10^{-3}	Martin et al. (2003)
R12	$HO_2 + dust \longrightarrow 0.5H_2O_2$	0.2	Zhu et al. (2010)
R13	$SO_2 + dust \longrightarrow SO_4^{2-}$	$1.0\times10^{-4} \sim 2.6\times10^{-4}$	Padnis and Carmichael (2000)

1

2

1 Table 3. Simulation Design

Scenario	Configuration of CMAQv5.0.1
Dust_Off	Without inline calculation of dust
Dust_Default	With default dust plume rise scheme
Dust_Revised	Revised initial friction velocity threshold constant in dust plume rise scheme
Dust_Profile	Same as Dust_Revised, but with implemented source-dependent speciation profile
Dust_Chem	Same as Dust_Profile, but with implemented dust chemistry with lower limit of uptake coefficient
Dust_ChemHigh	Same as Dust_Chem, but with upper limit of uptake coefficients

2

3

1 Table 4. Observations used in this study

Dataset	Species measured	Observational frequency	Number of sites	Data source
AERONET	AOD	Daily	70 sites within our simulation domain	http://aeronet.gsfc.nasa.gov/cgi-bin/combined_data_access_new
API	PM_{10}	Daily	86 cities in China	http://datacenter.mep.gov.cn
EANET	PM_{10}, SO_2, NO_x, HNO_3, O_3	Hourly/Daily/Bi-weekly	11 sites in Japan	http://www.eanet.asia/
Fudan Univ. Obs	K^+, Mg_2^+, Ca_2^+, $PM_{2.5}$	Daily (2006-2007)	Duolun (42.18°N, 116.48°E), Yulin (38.3°N, 109.77°E)	Huang et al. (2010)
MODIS	AOD	Daily	-	http://ladsweb.nascom.nasa.gov/data/search.html
TAQMN	PM_{10}	Daily	Xinzhuang (25.03°N,121.43°E)	http://taqm.epa.gov.tw/taqm/en/default.aspx

2
3

1 Table 5. Evaluation statistics for tracer metals and $PM_{2.5}$

	$PM_{2.5}$	K^+		Mg_2^+		Ca_2^+	
		Dust_Revised	Dust_Profile	Dust_Revised	Dust_Profile	Dust_Revised	Dust_Profile
Mean Obs ($\mu g/m^3$)	81.52	0.23		0.19		2.24	
Mean Sim ($\mu g/m^3$)	44.36	0.69	0.12	0.02	0.12	3.06	1.05
MB ($\mu g/m^3$)	-37.17	0.46	-0.11	-0.17	-0.07	0.82	-1.19
NMB (%)	-45.59	208.9	-47.83	-99.8	-36.84	36.69	-53.12
R	0.67	0.42	0.44	0.22	0.51	0.22	0.44

2

3

Table 6. CMAQ evaluation against EANET observations for Dust_Profile, Dust_Chem, and Dust_ChemHigh scenarios for species O_3, SO_2, SO_4^{2-}, NO_x, HNO_3, and NO_3^-

		O_3 (ppbv)	SO_2 (ppbv)	SO_4^{2-} ($\mu g/m^3$)	NO_x (ppbv)	HNO_3 (ppbv)	NO_3^- ($\mu g/m^3$)
Mean Obs		45.81	0.59	4.38	1.75	0.43	1.52
MB	Dust_Profile	0.59	0.54	-0.71	0.63	0.46	-0.20
	Dust_Chem	-0.92	0.42	0.60	0.67	0.36	-0.03
	Dust_ChemHigh	-2.07	0.38	1.29	0.68	0.35	0.37
NMB (%)	Dust_Profile	1.26	90.70	-16.28	35.61	109.03	-13.07
	Dust_Chem	-1.97	69.83	13.74	37.79	85.17	-1.97
	Dust_ChemHigh	-4.43	63.70	29.43	38.21	81.24	24.09
R	Dust_Profile	0.63	0.68	0.79	0.69	0.65	0.71
	Dust_Chem	0.62	0.65	0.75	0.69	0.59	0.72
	Dust_ChemHigh	0.59	0.64	0.72	0.69	0.60	0.73

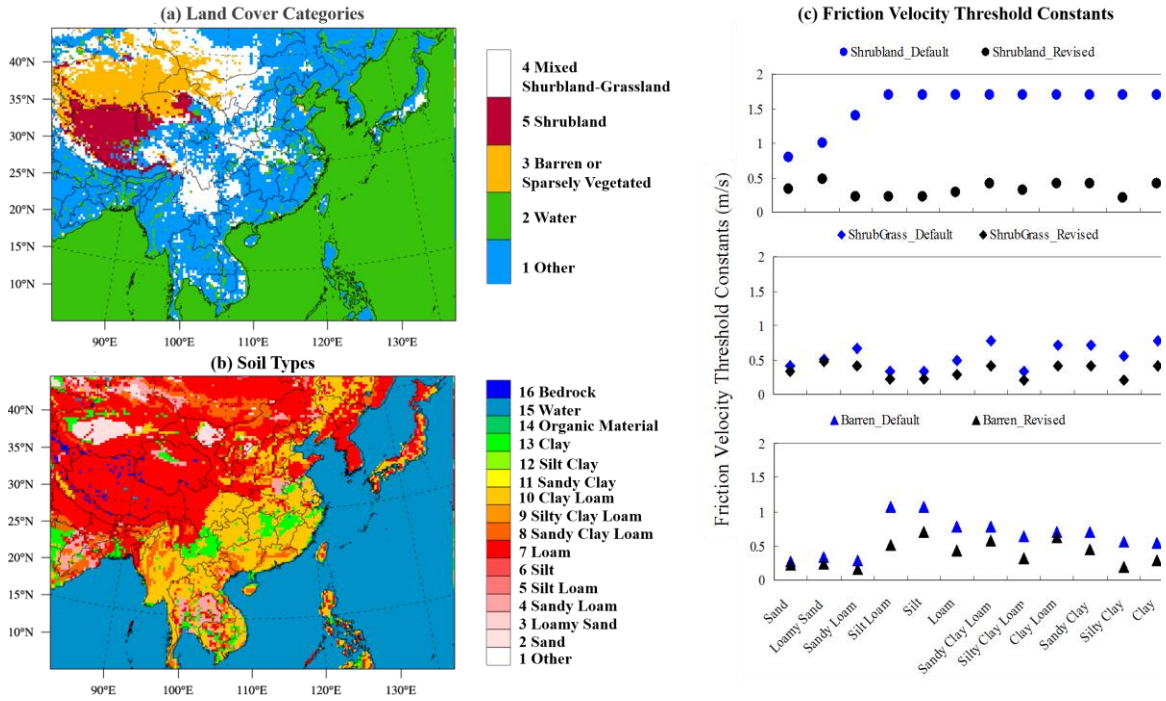

Figure 1. (a) Land cover categories, (b) Soil types, and (c) comparison of initial friction velocity threshold constants in default (blue markers) and revised (black markers) dust schemes for shrub land (top), mixed shrub and grassland (middle), and barren or sparsely vegetated (bottom) land cover.

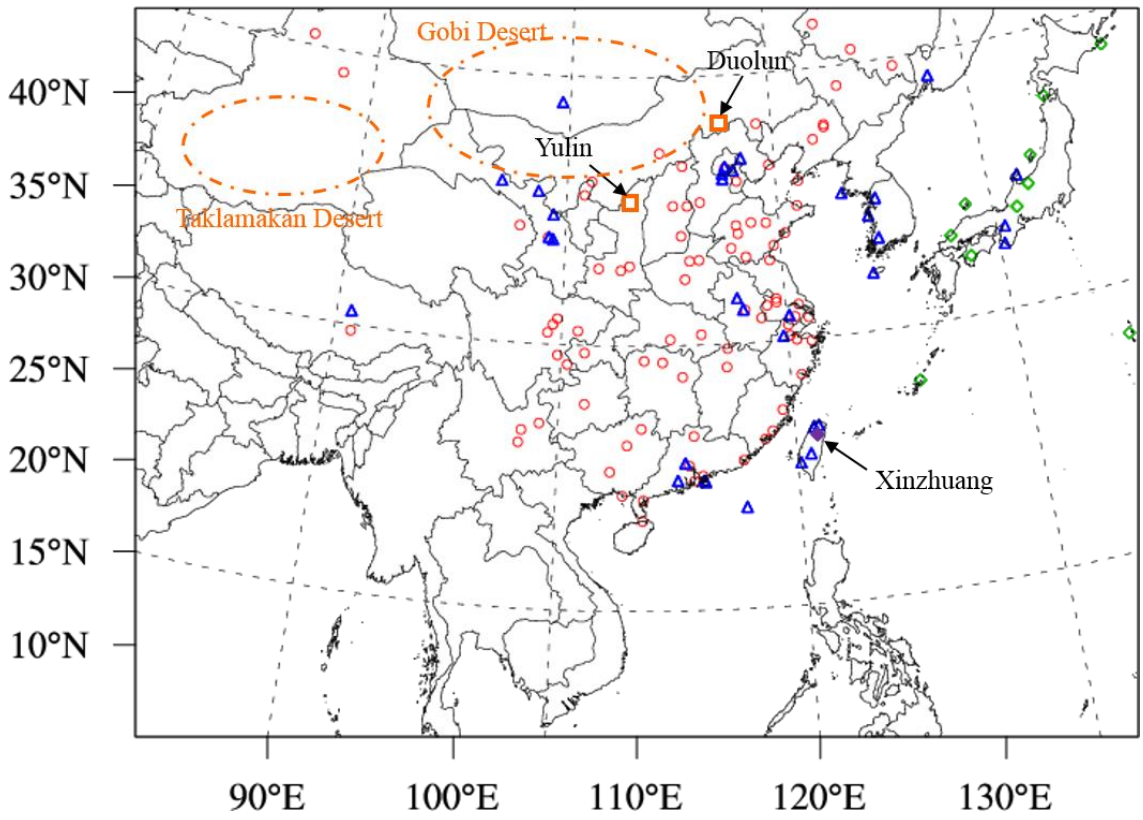

Figure 2. Modeling domain and locations of observation stations from Fudan observation (Duolun and Yulin indicated by orange rectangles), API (red circles), AERONET (blue triangles), EANET (green diamonds), and TAQMN (Xinzhuang indicated by purple diamond) over East Asia.

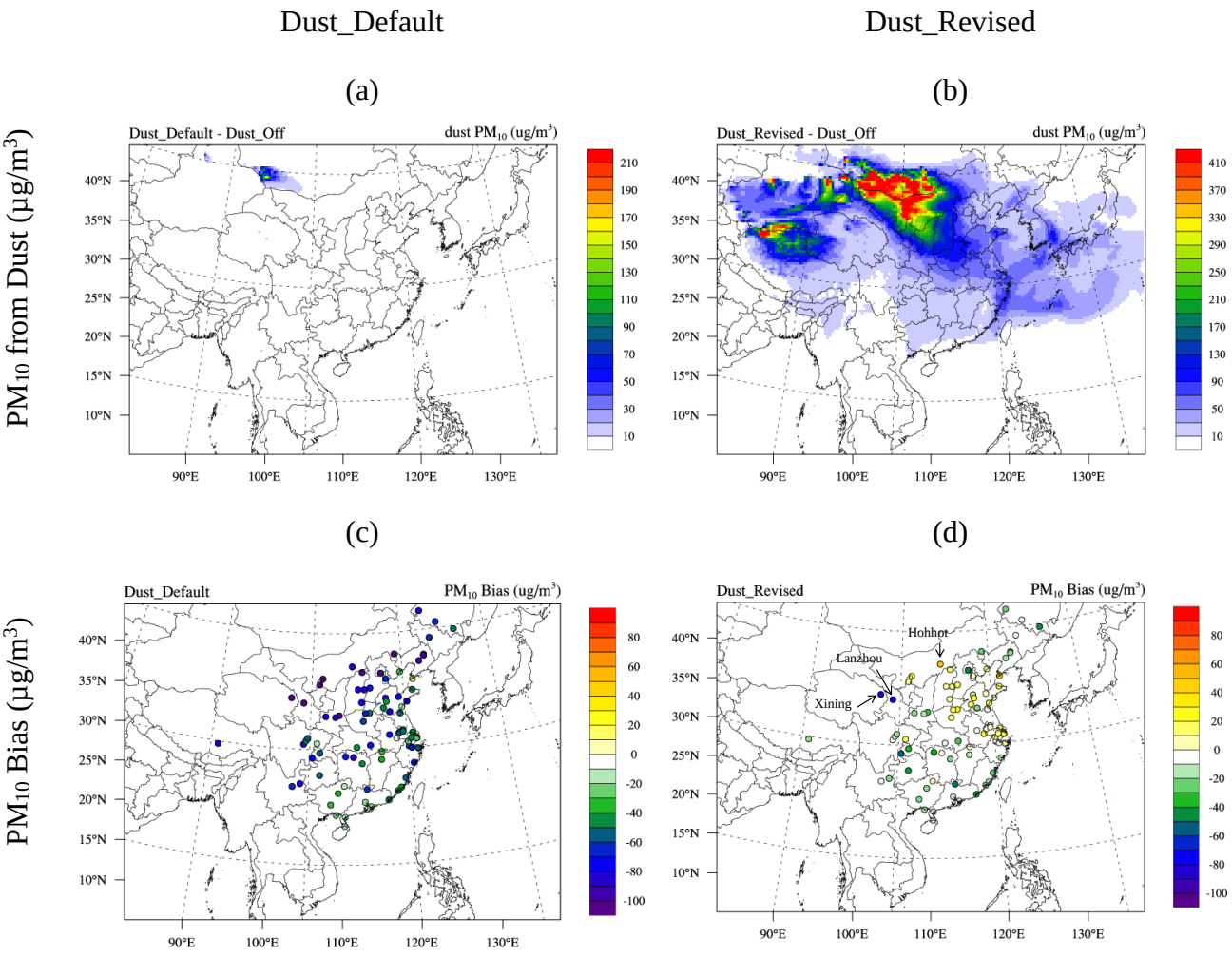

Figure 3. PM_{10} concentration difference from (a) Dust_Default - Dust_Off, and (b) Dust_Revised - Dust_Off. PM_{10} simulation bias against observation at API stations for (c) Dust_Default and (d) Dust_Revised scenarios.

1

(a) Dust_Off (b) Dust_Default (c) Dust_Revised

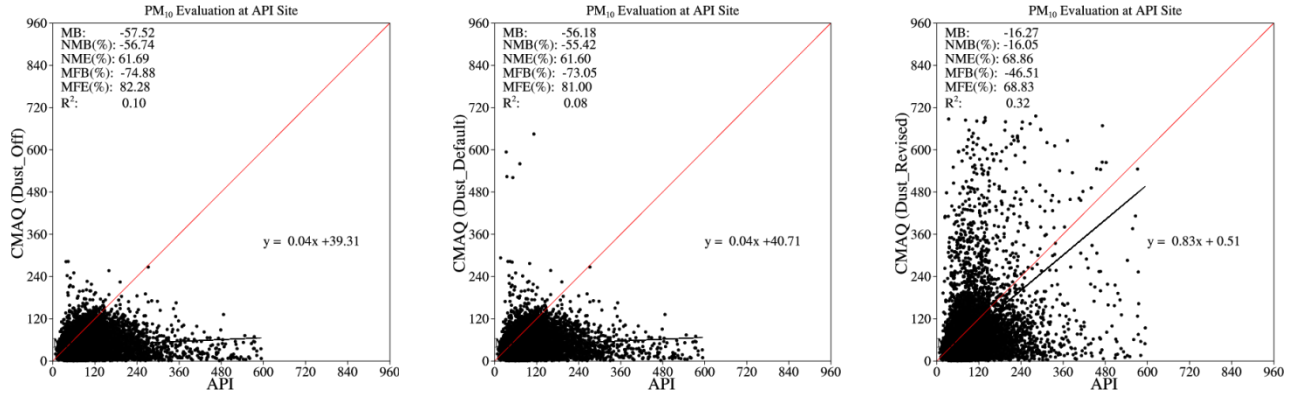

(d) Dust_Off (e) Dust_Default (f) Dust_Revised

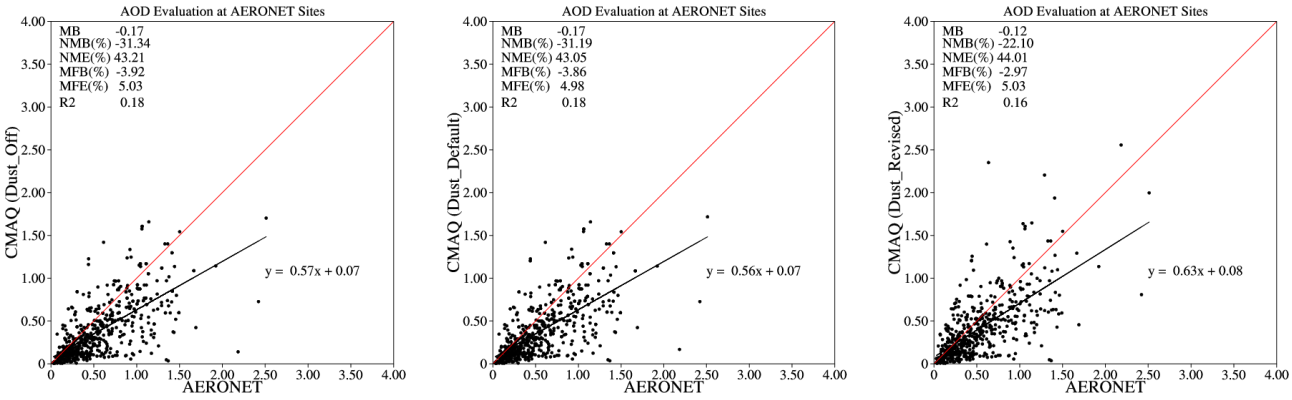

2

3 Figure 4. CMAQ evaluation against PM_{10} from API (upper row) and AOD (bottom row)
4 from AERONET for Dust_Off (left column), Dust_Default (middle column), and
5 Dust_Revised (right column) scenarios. Formula of calculating evaluation statistics
6 including mean bias (MB), normalized mean bias (NMB), normalized mean error (NME),
7 mean fractional bias (MFB), mean fractional error (MFE), and correlation coefficient (R)
8 can be found in Dong et al. (2013).

9

1

(a) Dust_Revised (b) Dust_Profile (c) $PM_{2.5}$

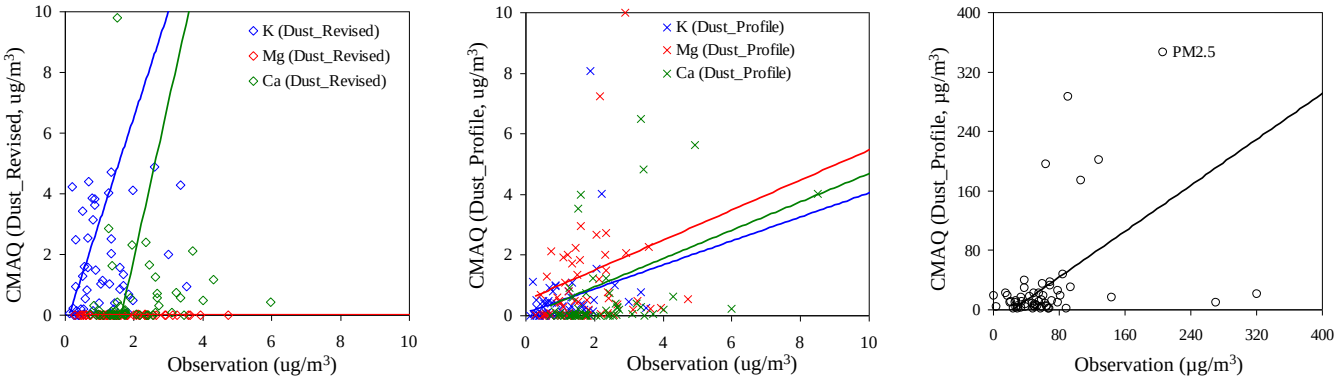

2

3 Figure 5. Model evaluations of CMAQ simulated metal tracers against observations from
4 Fudan University at Duolun and Yulin for (a) Dust_Revised and (b) Dust_Profile
5 scenarios. Note that simulations and observations of K^+ and Mg_2^+ are upscaled by 5
6 and 10 times, respectively, to make them comparable with Ca_2^+ in the same plot. Right
7 column is the evaluation of CMAQ simulated (c) $PM_{2.5}$ at Duolun and Yulin.

8

1

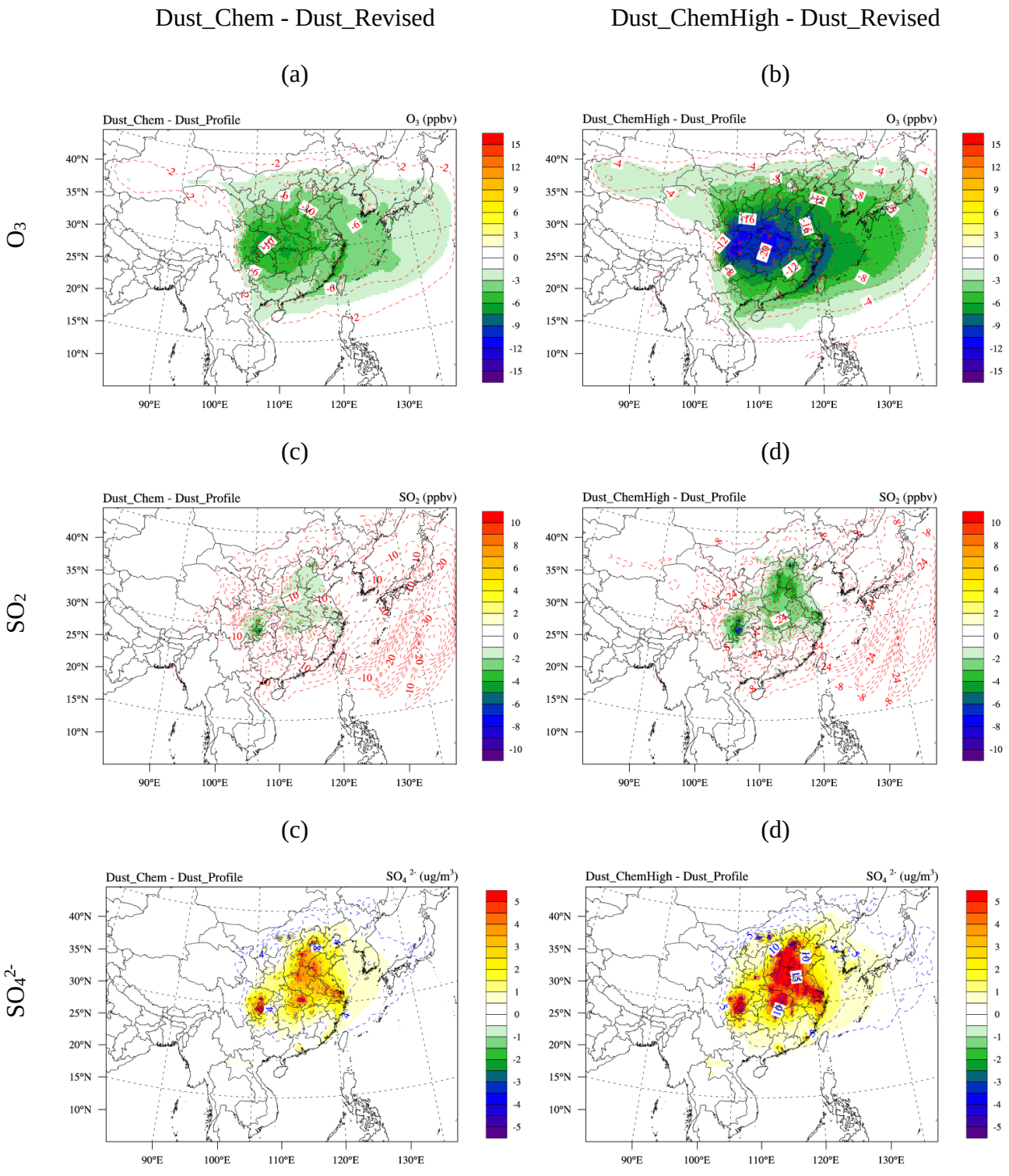
Dust_Chem - Dust_Revised
Dust_ChemHigh - Dust_Revised
(a)
(b)
(c)
(d)
(c)
(d)
O3
SO2
SO4 2-
Dust_Chem - Dust_Profile
Dust_ChemHigh - Dust_Profile
O3 (ppbv)
SO2 (ppbv)
SO4 2- (ug/m3)
90°E
100°E
110°E
120°E
130°E
10°N
15°N
20°N
25°N
30°N
35°N
40°N

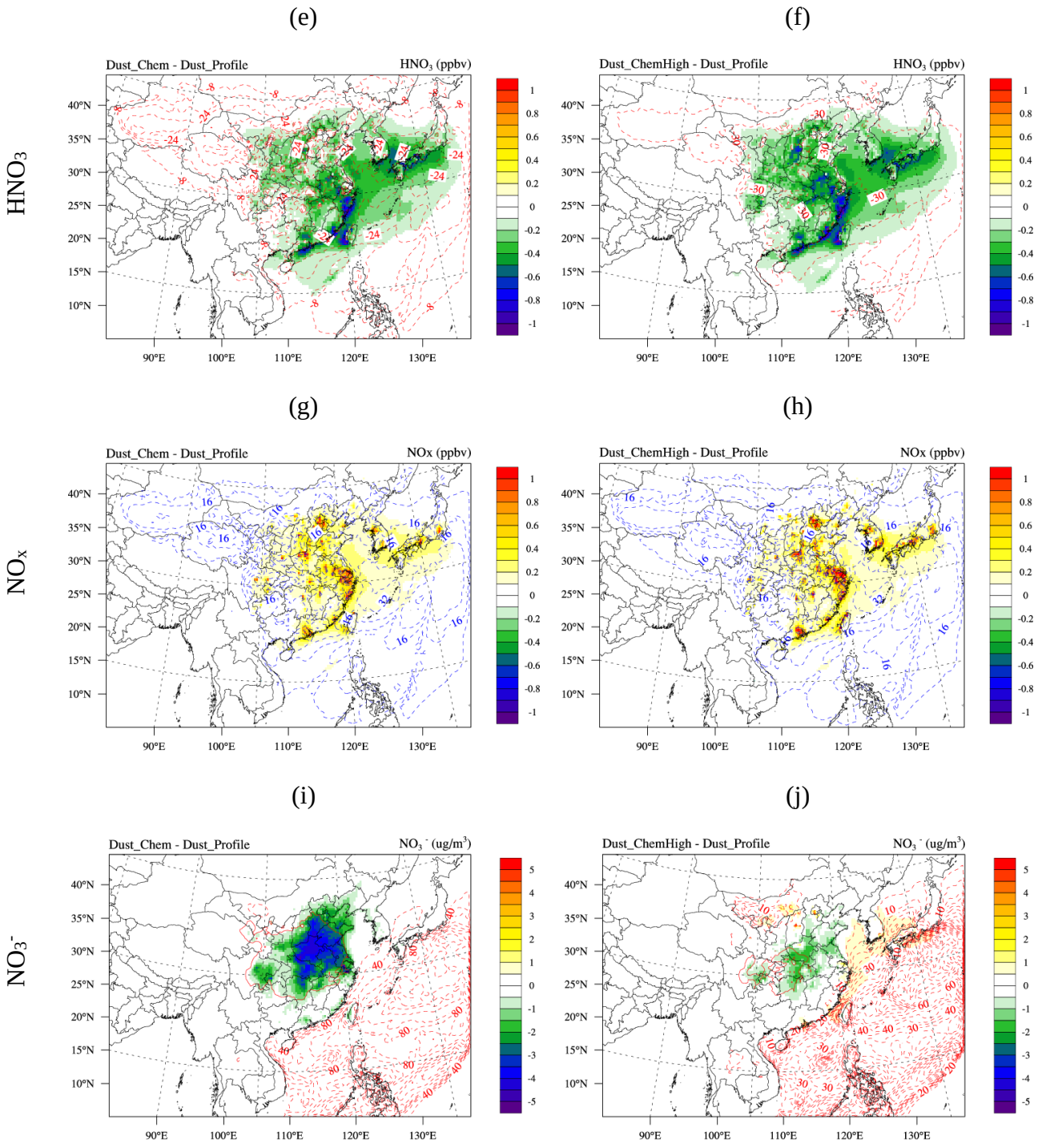

1

2 Figure 6. Five-year averages for March and April from 2006 to 2010 of dust

3 heterogeneous chemistry impacts with lower (left column) and upper (right column)

4 uptake coefficients, for species O_3 (1st row), SO_2 (2nd row), SO_4^{2-} (3rd row), HNO_3 (4th

row), NO_x (5^{th} row), and NO_3^- (6^{th} row). Color contours represent the absolution concentration changes, and dash contour lines with numbers indicate the percentage changes.

MODIS

CMAQ

(a) Mar.19th 2010

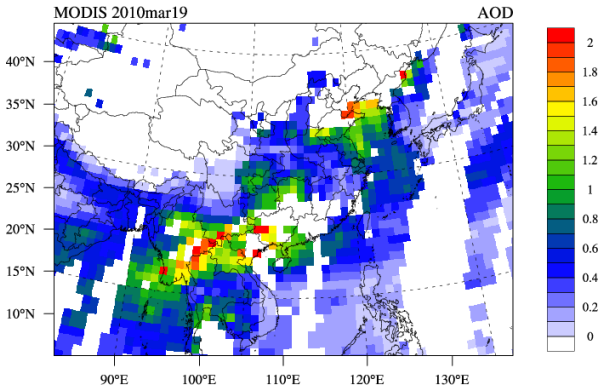

(b) Mar.19th 2010

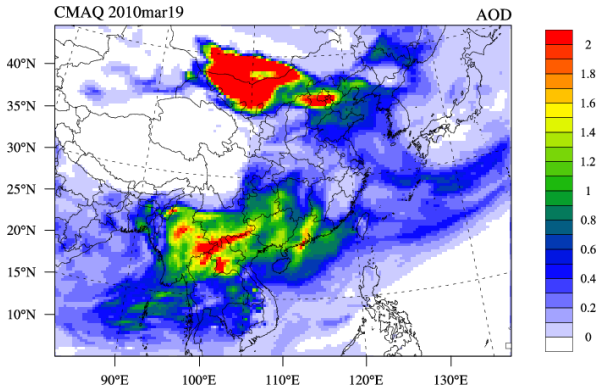

(c) Mar.20th 2010

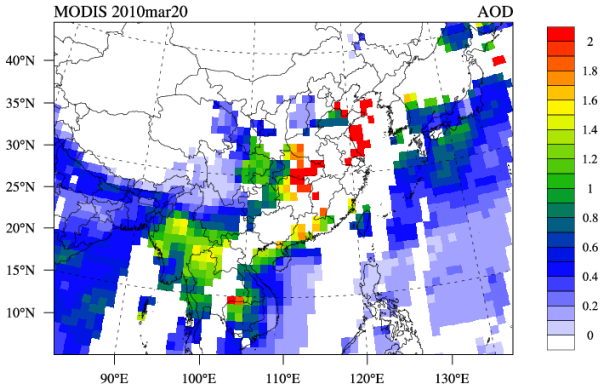

(d) Mar.20th 2010

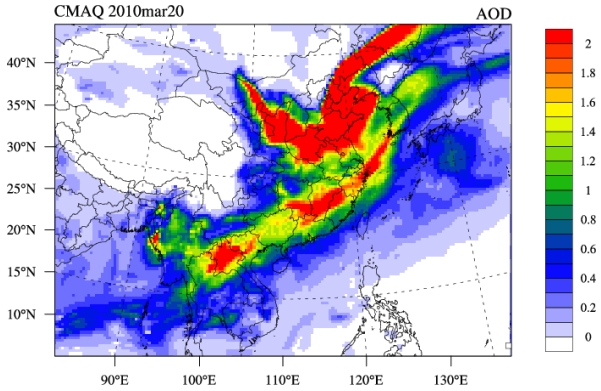

(e) Mar.21st 2010

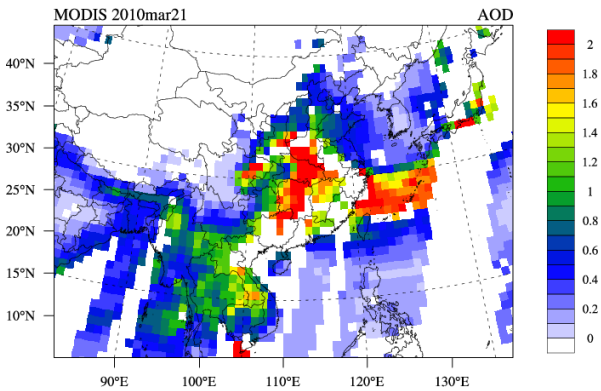

(f) Mar.21st 2010

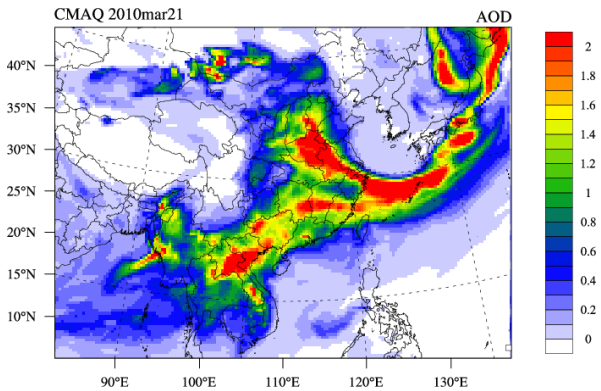

1

Figure 7. Daily MODIS observed (left column) and CMAQ simulated AOD (right column) for March 19th (top row), March 20th (middle row), and March 21st (bottom row).

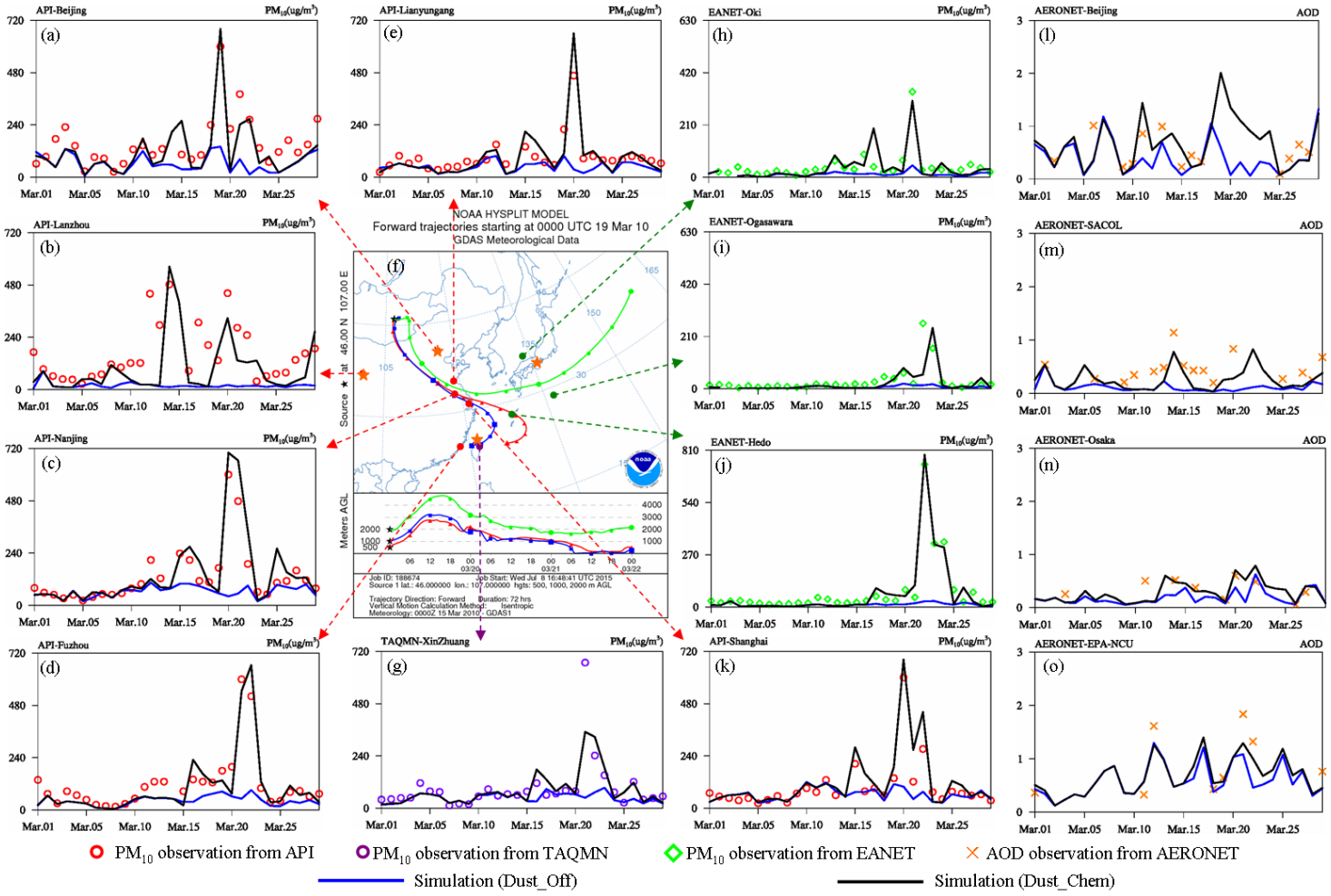

Figure 8. Forward trajectories from (f) HYSPLIT, and temporal variations of PM_{10} and AOD on a daily scale. Comparison between simulated (black lines for Dust_Chem scenario, and blue lines for Dust_Off scenario) and observed PM_{10} from API (red circles) at (a) Beijing, (b) Lanzhou, (c) Nanjing, (d) Xiamen, (e) Lianyungang, and (k) Shanghai. Comparison between simulations and observed PM_{10} from TAQMN (purple circles) at (g) Xinzhuang. Comparison between simulations and observed AOD from EANET (green diamonds) at (l) Beijing, (m) SACOL, (n) Osaka, and (o) NCU. Locations of cities or stations are indicated by the tails of arrow lines (for PM_{10}) or orange stars (for AOD)

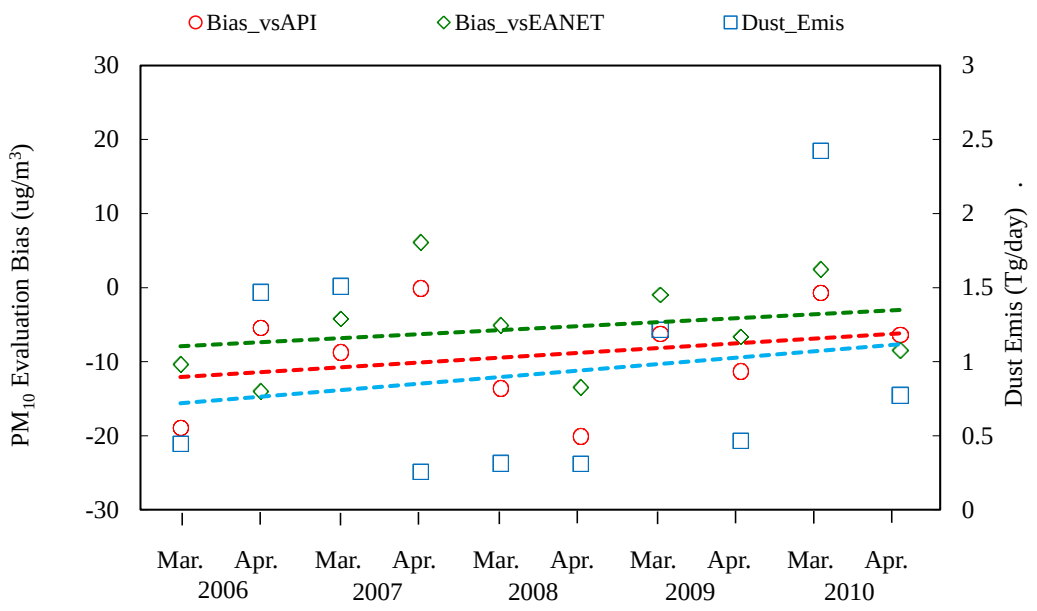

Figure 9. CMAQ predictions of dust emission rate (solid orange rectangles), and simulation bias of PM_{10} against observations from API (red circles) and EANET (green diamonds). Dash lines indicated the trends of the variables.

(a) FNL soil moisture fraction (b) GLDAS soil moisture fraction

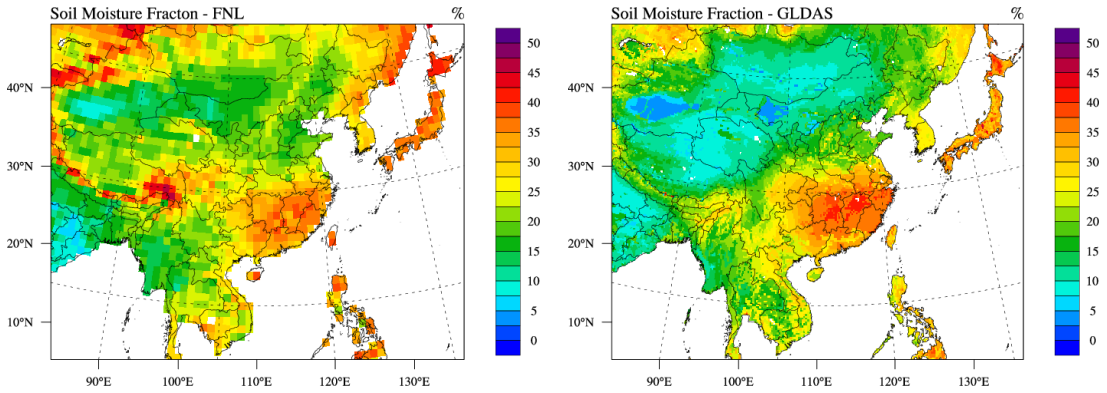

Figure 10. Five-year averages (for March and April) of soil moisture fraction in top 10cm soil depth from (a) FNL and (b) GLDAS.